Title
The Mechanism of Processivity and Directionality of Cytoplasmic Dynein

Author
Cleary, Frank Banta

Publication Date
2014

Peer reviewed|Thesis/dissertation

The Mechanism of Processivity and Directionality of Cytoplasmic Dynein

By

Frank Banta Cleary

A dissertation submitted in partial satisfaction of the requirements for the degree of

Doctor of Philosophy

in

Biophysics

in the

Graduate Division

of the

University of California, Berkeley

Committee in charge:

Professor Ahmet Yildiz, Chair
Professor Eva Nogales
Professor Carlos Bustamante
Professor Georjana Barnes

Spring 2014

Abstract

The Mechanism of Processivity and Directionality of Cytoplasmic Dynein

By

Frank Banta Cleary

Doctor of Philosophy in Biophysics

University of California, Berkeley

Professor Ahmet Yilidz, Chair

Cytoplasmic dynein is a dimeric motor that transports intracellular cargoes towards the minus-end of microtubules (MTs). In contrast to other processive motors, microtubule release of the dynein heads is not precisely coordinated and the mechanism of dynein processivity remains unclear. By engineering the mechanical and catalytic properties of the motor we show that dynein processivity minimally requires a single active motor domain (head) and a second inert MT binding domain. The AAA+ ring and the linker of the other head are dispensable, suggesting that processivity arises from a high ratio of MT bound to unbound time, and not from interhead communication. Additionally, nucleotide-dependent microtubule release is gated by tension on the linker domain.

We find that dynein releases rapidly from the MT when force is applied in the forward direction (towards the minus-end), but remains bound under backward forces. This finding suggests that the asymmetric release properties of the microtubule binding domain (MTBD) control dynein directionality. Consistent with this hypothesis, replacing the MTBD with a catalytically inactive kinesin motor domain, which favors release towards the plus end, results in reversal of motor directionality. Furthermore, a dynein dimer maintains its minus-end directed motility when the released monomer is allowed to orient freely during the search for a new binding site. The results rule out directionality models based on a swinging mechanism of the linker domain. We propose that the mechanism of dynein directionality is fundamentally distinct from kinesin and myosin motors and determined by asymmetric release and binding properties of its MT binding interface. We develop a quantitative model for dynein stepping that reproduces the velocity and stepping characteristics of dynein motors and their response to chemical and mechanical perturbation.

Table of Contents

Acknowledgements

I'm grateful to the many people who assisted in making this work possible. I particularly want to acknowledge those whose scientific and technical contributions helped shape the course of my research, including Tom Bilyard, Zaw Htet, Andrew Carter, Vladislav Belyy, Jigar Bandaria, Helgo Schimdt, Danna Chan, Amy Chang and Ahmet Yildiz.

I began doing lab work at Cornell University where Barbara Baird, Dave Holowka, and Sarah Veatch helped to train me so that I was prepared with the necessary experience in scientific thought to design and implement many of the experiments that became this thesis.

On a personal note I'd like to thank my parents, Joy Veronneau and Richard Cleary, who encouraged me to pursue a Ph.D. and helped support my education. I am very grateful to my wife, Lea Cleary, whose advice, scientific input, and encouragement toward excellence allowed me to achieve much more than I could have alone. My thesis work benefited greatly from her constant support.

Introduction

Cytoplasmic dynein (herein dynein) is a processive microtubule motor involved in a wide range of cellular functions. Dynein transports membrane-bound organelles, vesicles and viruses towards the MT minus end (Vallee et al., 2004) and plays important roles in mitosis, including positioning the spindle (Carminati and Stearns, 1997), focusing the MTs into poles (Morales-Mulia and Scholey, 2005), and regulating the spindle assembly checkpoint (Griffis et al., 2007). Impaired dynein function has been implicated in motor neuron degeneration (Hafezparast et al., 2003), lissencephaly and primary ciliary dyskinesia (Gerdes and Katsanis, 2005).

Dynein consists of a homodimer of two large (~520 kDa) heavy chains which contain six concatenated AAA+ ATPase subunits arranged in a hexameric ring ~15 nm in diameter (Figure 1A) (Kon et al., 2012; Roberts et al., 2009; Schmidt et al., 2012). Only the N-terminal four AAA subunits retain ATPase motifs; hydrolysis at AAA1 is essential for motility and ATPase mutations at AAA3 severely reduce motor velocity (Cho et al., 2008; Kon et al., 2004). Unlike kinesin, whose MT binding and ATPase sites are part of the same globular domain, dynein's MT-binding domain (MTBD) is separated from the ring by a ~15 nm coiled-coil stalk (Gee et al., 1997). The linker domain has been proposed to drive motility by shifting its position across the ring, coupled to the ATPase activity of AAA1 (Burgess et al., 2003; Kon et al., 2005; Roberts et al., 2009). Dynein's N-terminal tail domain dimerizes the heavy chains and forms a complex with a variety of non-catalytic subunits (Figure 1B)(Kardon and Vale, 2009). The dynactin complex mediates cargo binding (Vallee et al., 2012), LIS1 and NudE/NudEL (Sasaki et al., 2000) regulate motor activity (McKenney et al., 2010).

Compared to processive kinesins and myosins, the mechanism of dynein motility remains elusive due to its large size and complex architecture. Kinesin-1 and myosin V walk hand-over-hand (Asbury et al., 2003; Yildiz et al., 2003, 2004), in which the leading head stays bound to the track while the trailing head takes a step. In kinesin-1, intramolecular tension (Yildiz et al., 2008) and the orientation of the linker domains (Clancy et al., 2011) were proposed to coordinate the stepping cycle of the heads. In contrast, dynein's heads are not strictly gated (DeWitt et al., 2012; Qiu et al., 2012), suggesting that each monomer can act independently of the other.

It remains unclear how the two heads are able to take many steps without dissociating from the MT in the absence of tight interhead communication. Dynein's distinct stepping mechanism suggests that it has different requirements for processive movement from kinesin and myosin, but the extent of this has not been investigated. The release of a dynein motor domain from an MT is initiated by ATP binding (Imamula et al., 2007), or can be facilitated by load without nucleotide (Gennerich et al., 2007). At high interhead separations the trailing head is more likely to take a step (DeWitt et al., 2012; Qiu et al., 2012); suggesting that the forward stepping rate of a head is increased under tension. Understanding how ATP- and force-dependent stepping pathways contribute to the motility of a dynein dimer is a major focus of this work.

Evidence that an ATP-dependent linker swing could power dynein motility is observed in electron micrographs (Burgess et al., 2003; Roberts et al., 2009), solution FRET (Kon et al., 2005) and filament gliding assays (Reck-Peterson et al., 2006; Shima et al., 2006a) on truncated

monomeric dyneins. However, the role of linker swing has not been tested on the motility of active dynein dimers. The linker makes multiple contacts with the ring and mutation of these contact sites significantly reduces ATPase activity (Kon et al., 2012; Schmidt et al., 2012). The conformation of the linker also correlates with the MT affinity of the motor (Imamula et al., 2007). Therefore, in addition to functioning as a lever arm, the linker may regulate nucleotide binding and the MT affinity of the motor, and facilitate communication between the heads.

In this work, how the mechanical and catalytic properties of the motor contribute to dynein processivity was investigated by engineering *S. cerevisiae* dynein constructs and testing their motility at a single molecule level (Figures 1C and 2). It was found that dynein motility is driven by nucleotide-dependent action of the linker, and a rigid attachment between the linkers is not required. Processivity minimally requires the linker domain of one active monomer to be attached to an inert MT tether retaining only the MT-binding domain. Dynein monomers have a strong tendency to release towards the MT minus-end under load and the release rate is increased by addition of ATP. Unexpectedly, exerting forces on dynein through the linker fully abolishes ATP-dependent MT release. Synthesizing our experimental results with high-resolution tracking studies, a computational model was developed to provide insight into the minus-end directionality and uncoordinated stepping of dynein.

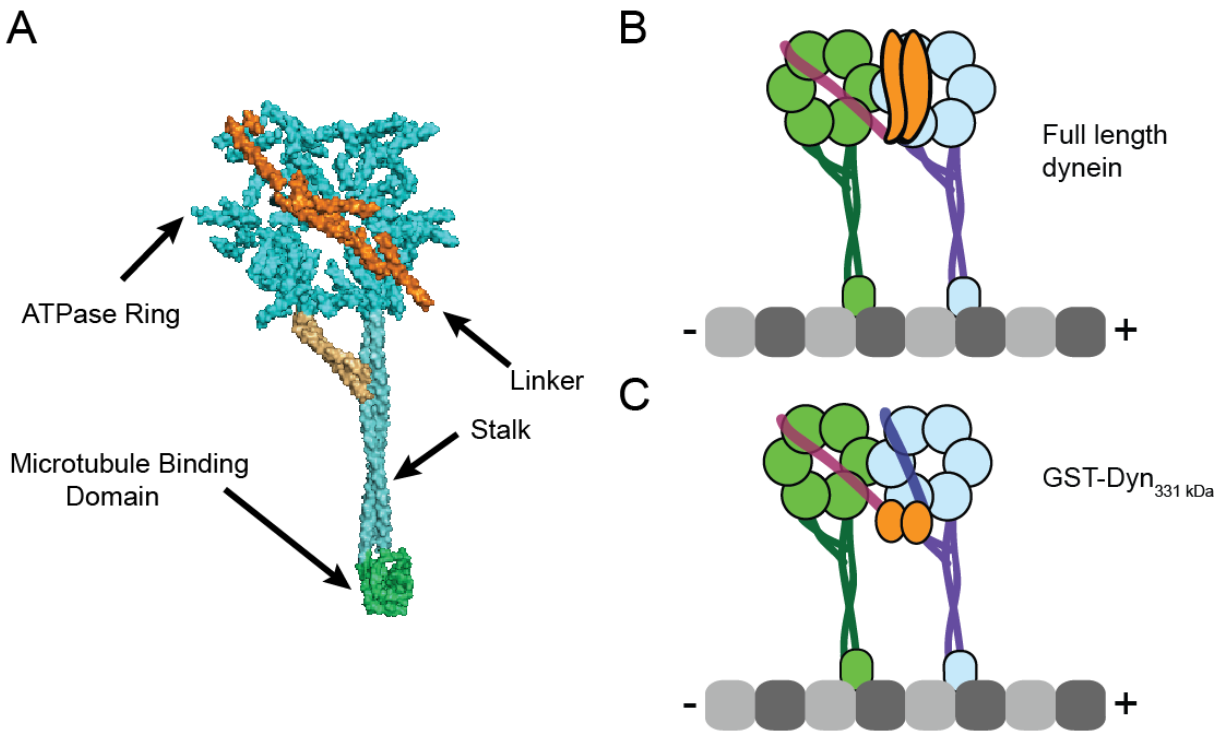

Figure 1.The structure of cytoplasmic dynein. (A) An X-ray diffraction structure showing the overall architecture of a dynein monomer, false colored to highlight notable domains (structure data from (Kon et al., 2012)). (B) A cartoon of the full length dynein dimer on a MT. (C) Throughout this work a truncated, artificially dimerized construct with similar biophysical properties to full length dynein (Reck-Peterson et al., 2006) has been used.

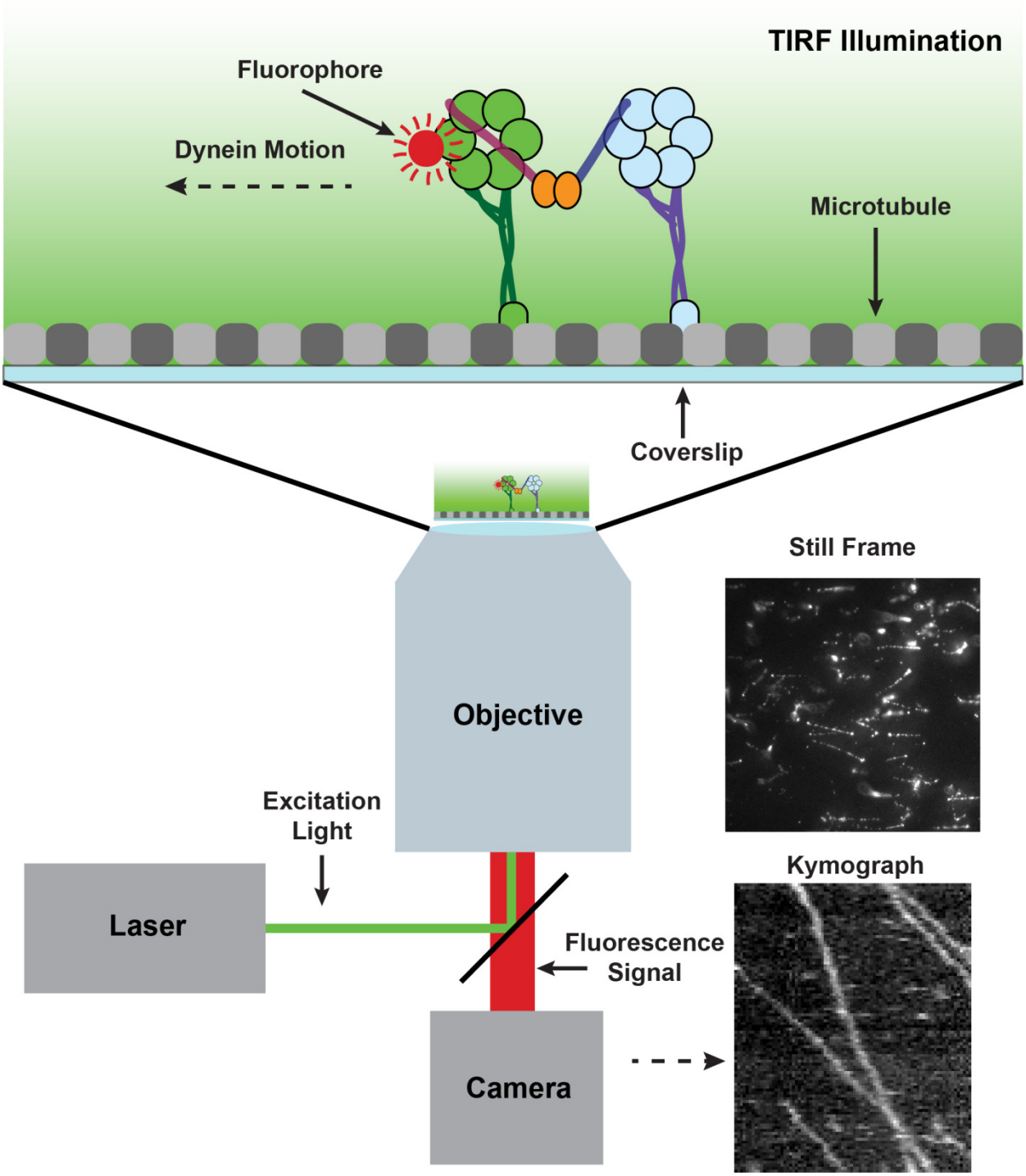

Figure 2. A schematic of the fluorescence assay used to measure dynein motor properties.

Chapter 1. A rigid connection between monomers is not required for dynein processivity.

Interhead tension is proposed to mediate the highly coordinated movement of the motor domains in kinesins and myosins. Reducing tension through peptide insertions affects kinesin velocity, processivity and efficiency of converting ATP hydrolysis into motion (Shastry and Hancock, 2010; Yildiz et al., 2008), and decreases myosin VI processivity (Dunn et al., 2010). It has remained unclear if reducing the rigidity of the linker domains affects the motility of dynein, whose heads are not strictly coordinated (DeWitt et al., 2012; Qiu et al., 2012).

To investigate the importance of a rigid linkage between monomers, a flexible peptide chain was inserted between the N-terminus of a truncated *S. cerevisiae* dynein monomer ($Dyn1_{331kD}$, Figure 1C) and a glutathione-S-transferase dimerization tag (GST-$Dyn1_{331kD}$, Figure 3). The GST-$Dyn1_{331kD}$ dimer has similar stepping behavior and processivity to that of the full-length dynein motor (Reck-Peterson et al., 2006). Because of the large size (~30 nm) of the dynein head, we chose longer peptides than the 4-10 nm contour length inserts used in myosin (Dunn et al., 2010) and kinesin (Yildiz et al., 2008) to reduce tension that may exist between the two monomers. We used a disordered insert consisting of glycine-serine repeats (GS) of varying lengths (12, 24 and 48 (GS) with contour lengths of 9.1, 18.2, and 36.5 nm, and average end to end distances of 2.9, 4.2 and 6.0 nm, respectively (Yildiz et al., 2008)). The (GS) inserts are expected to provide a soft connection between the monomers.

The movement of extended dyneins was visualized by total internal reflection fluorescence (TIRF) microscopy (Figure 2). Despite the altered mechanics of the linker domain, we observed that the GS insertion mutants moved processively, on average taking more than 100 steps without dissociating from the MT (Figure 3). Unlike engineered kinesin and myosin motors with flexible inserts, the mean velocity and run length of the (GS) insertion dynein mutants were similar to those of GST-$Dyn1_{331kD}$ (Figure 3). The results show that rigid mechanical coupling between the heads through the linker domains is not essential for dynein motility. The linker domain of native dynein may have flexible regions (Kon et al., 2012; Schmidt et al., 2012), explaining why further mechanical uncoupling of the linkers does not affect dynein velocity and processivity.

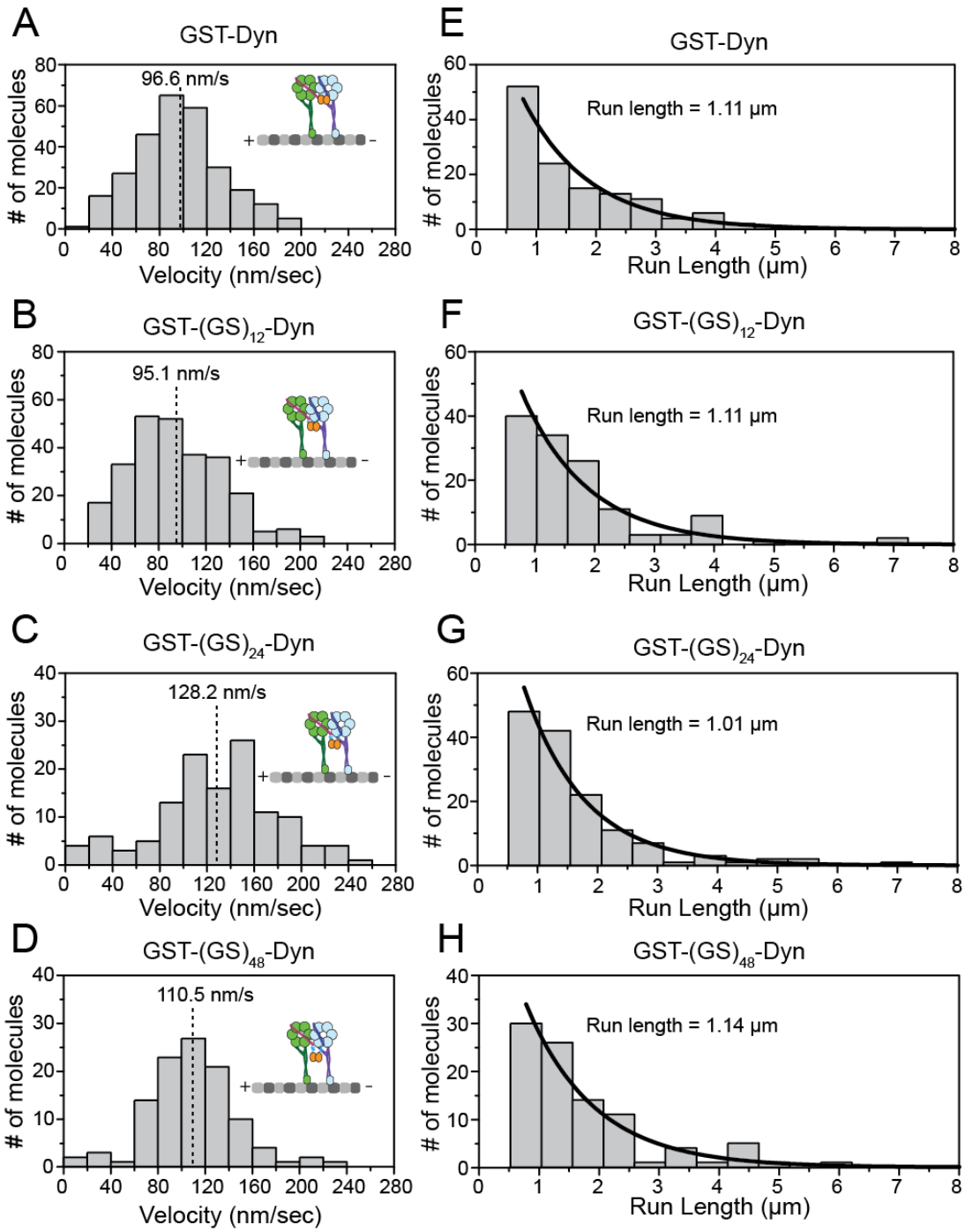

Figure 3. The addition of a flexible linkage between monomers does not affect dynein velocity or run length. The speed (A-D) and run length (E-H) histograms of the (GS) insertion mutants. Dynein mutants with $(GS)_{12}$ (B, F), $(GS)_{24}$ (C, G), and $(GS)_{48}$ (D, H) inserts between the GST dimerization tag and the linker have comparable speed and processivity to GST-Dyn_{331kD}.

Chapter 2. Dynein motility requires only one active monomer

The role of the distinct ATPase sites in dynein motility is not well established. ATPase mutations at the AAA1 site disrupt the linker swing mechanism (Kon et al., 2005) and abolish the motility of a dynein homodimer; AAA3 mutant homodimers move ten-fold slower than native dynein (Cho et al., 2008; Kon et al., 2004). Using a fluorescence based assay, the nucleotide dependent release of $Dyn1_{331kD}$ monomers from surface-immobilized MTs was measured (Huang et al., 2012) (Figure 4). To study how ATPase activity affects this process, we inserted an ATP binding deficient K/A mutation in the Walker A motif or a hydrolysis deficient E/Q mutation in the Walker B motif at the AAA1 or AAA3 sites. Consistent with the biochemical assays on *Dictyostelium* dynein (Imamula et al., 2007), we observed that wild-type (WT) and $AAA1_{E/Q}$ (E1849Q) $Dyn1_{331kD}$ monomers release from MTs in the presence of ATP, while $AAA1_{K/A}$ (K1802A) monomers remain strongly bound (Figure 4). WT monomers do not release in the absence of nucleotide or in the presence of the non-hydrolyzable ATP analog AMP-PNP.

We tested the effect of these ATPase mutations when present on a single monomer of a dynein dimer constructed with FRB-FKBP12 heterodimerization tags (Figure 5B; Table 1) (Banaszynski et al., 2005; Reck-Peterson et al., 2006). A heterodimer of FRB-$Dyn1_{331kD}$ and FKBP12-$Dyn1_{331kD}$ ("WT/WT") moves at slightly reduced velocity and processivity compared to GST-$Dyn1_{331kD}$ (Figures 3A, 5C) (Reck-Peterson et al., 2006). When single ATPase mutations were introduced to a monomer, the largest effects on motility were observed in AAA1 mutants. Compared to WT/WT, $AAA1_{E/Q}$/WT heterodimers had a ~20% reduced velocity and run length, while $AAA1_{K/A}$/WT motors had a ~60% reduction in velocity and a 200% increase in run length (Figure 5C,D,E). These results indicate that a WT monomer can pull an inactive AAA1 mutant head faster when it has a reduced MT affinity, at the expense of reduced processivity. $AAA3_{K/A}$/WT (K2424A) and $AAA3_{E/Q}$/WT (E2488Q) heterodimers showed a similar reduction in motor velocity to $AAA1_{K/A}$/WT (Figure 5C), suggesting that ATPase activity at AAA3 may regulate the AAA1 site.

The velocity of the mutant heterodimers is linearly related to the probability of a processive run ending per unit time (Figure 5E). The WT head can pull its inactive partner faster when it has a reduced MT affinity (e.g. AAA1E/Q), but these constructs are less processive than those where the mutant head is locked in a state with high affinity to MT. The results suggest that the magnitude of dynein processivity is determined by the duty ratio (the ratio of MT bound to unbound time in a stepping cycle) of each head, not by the precise coordination of the stepping cycles of the heads (DeWitt et al., 2012; Qiu et al., 2012).

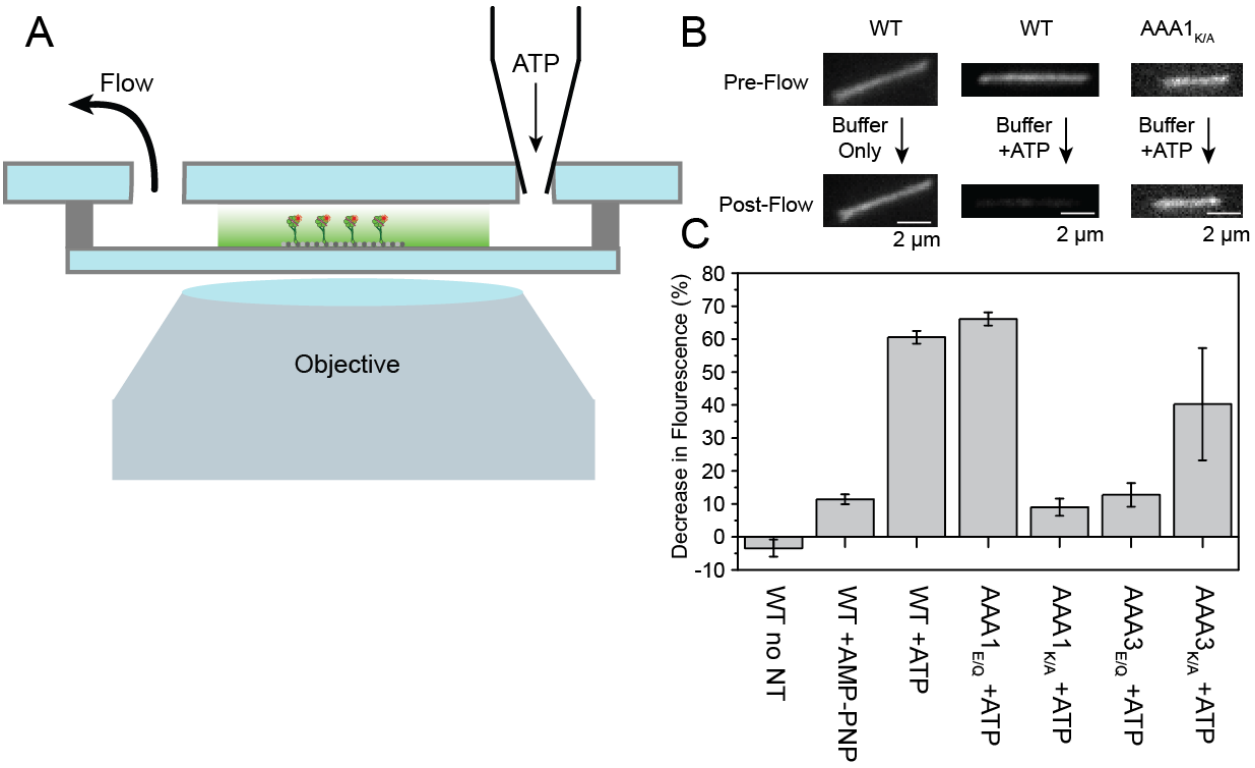

Figure 4. ATP-dependent release of dynein monomers from MTs in the absence of load. (A) A schematic of the nucleotide-flow assay. A sample containing surface-immobilized MT filaments sparsely decorated with fluorescently-labeled dynein monomers. During data acquisition, the sample is washed with solution containing nucleotide. (B) Cropped images showing a MT before and after ATP flow for WT (buffer only and with ATP), and $AAA1_{K/A}$ mutant dynein monomers. (C) The normalized decrease in fluorescence (i.e. the fraction of monomers released) for different mutants and nucleotide conditions (errors bars: SEM). WT monomers remain stably-attached to MT in the absence of nucleotide and in 2 mM AMP-PNP (non hydrolyzable ATP analogue which triggers ATP bound state). Upon introduction of 2 mM ATP, 65% of WT monomers release from the MT within 0.2 s. $AAA1_{E/Q}$ mutants also show ATP-dependent MT release in similar quantity to WT monomer. In contrast, $AAA1_{K/A}$ mutants show minimal release from MTs in the presence of ATP, similar to the WT monomer in 2 mM AMP-PNP. $AAA3_{E/Q}$ and $AAA3_{K/A}$ mutants also display defects in ATP-dependent MT release, compared to WT monomer, suggesting a regulatory role for AAA3 site in MT binding affinity of dynein MTBD-stalk.

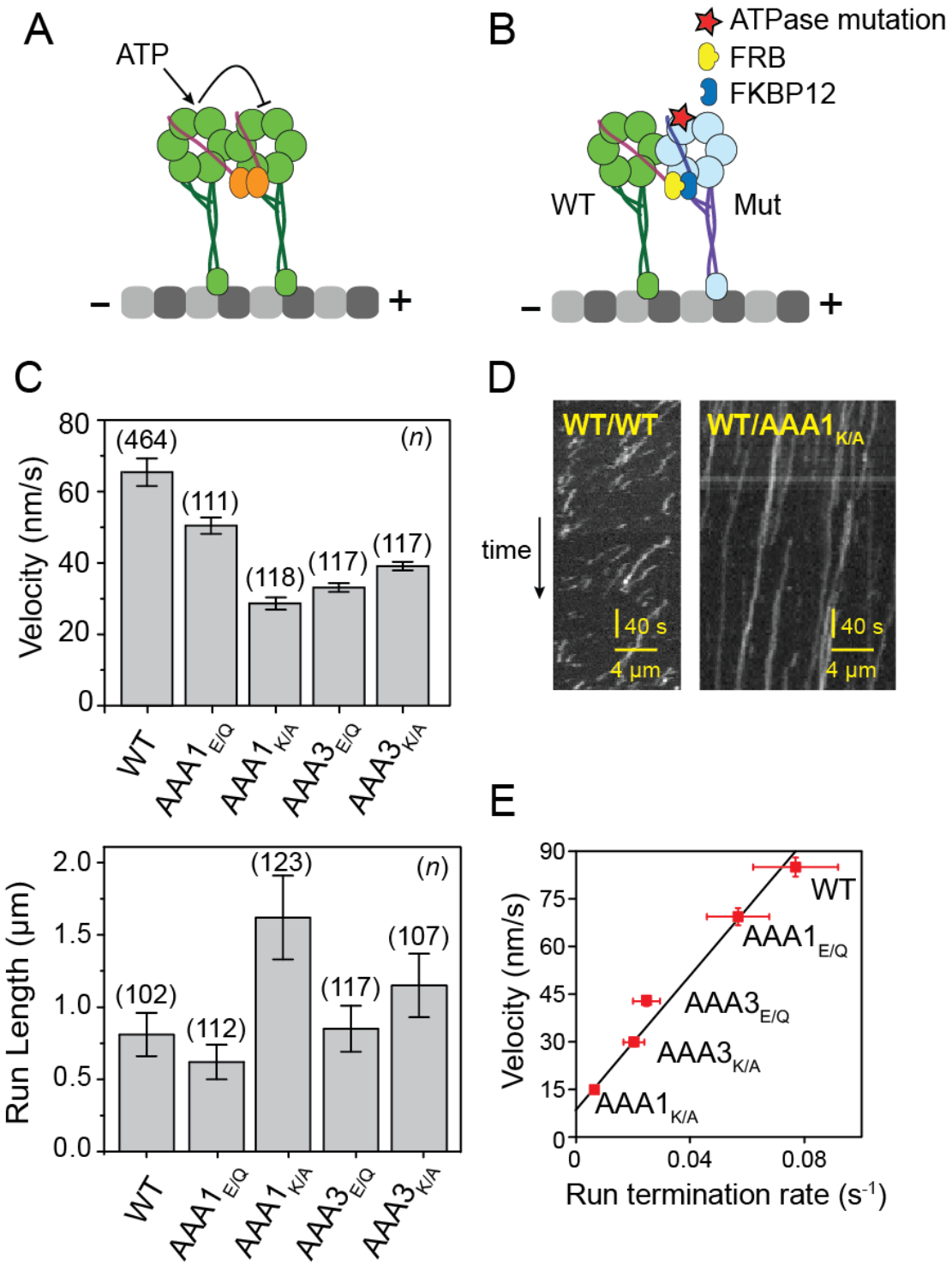

Figure 5. Motile properties of heterodimeric dynein constructs bearing a single ATPase mutation. (A) The nucleotide gating model requires the ATPase cycles of the two heads to be kept out of phase. (B) A schematic (right) of FRB-FKBP12 dynein heterodimer on a MT. (C) Average velocity (± SEM) and run length (± 95% CI) of TMR labeled dynein motors at 2 mM ATP. One WT monomer is dimerized with a partner carrying the indicated ATPase mutation. (D) Kymographs showing the processive movement of WT/WT and WT/AAA1$_{K/A}$ motors. (E) Plot of velocity vs. run termination rate for the indicated heterodimers shows a linear relationship (black line).

Chapter 3. Linker-linker dimerization is not required for dynein motility and the linker domain is a mechanical element that powers dynein motility

To understand the role of the linker swing in driving dynein motility, a heterodimer composed of two catalytically identical but mechanically distinct monomers was engineered. One of the monomers was tagged with FRB at the N-terminal linker and the other monomer contained a C-terminal FKBP12 tag. Heterodimerization of these monomers leads to a one bound-linker head (BLH, N-terminal heterodimerization domain) and one free-linker head (FLH, C-terminal heterodimerization domain) (Figure 6A).

Motility assays revealed that the FLH/BLH heterodimer moves processively towards the minus end of MTs. FLH/BLH motors moved at 85% of the velocity of the WT/WT heterodimer (Figure 6B). Intriguingly, the run length of FLH/BLH (2.25 ± 0.41 μm; mean ± 95% confidence interval) was more than double that of WT/WT (Figure 6C). The results show that N-terminal dimerization is not essential for processive motion and alternative dimerization geometries can achieve increased processivity with a minor reduction in motor velocity.

We next examined whether each head contributes to driving motility in the FLH/BLH heterodimer. According to the powerstroke model (Roberts et al., 2009), in order to generate force a head must be attached to the other head through its linker domain, either to push against the other head or to pull it forward. Therefore, inhibiting the linker swing in the BLH would be predicted to abolish motility, while motors with an inhibited FLH would remain motile.

To test whether the linker is the mechanical element that drives processive motility, we disrupted the linker swing mechanism of one head by introducing AAA1 ATPase mutations (Kon et al., 2005). AAA1 mutations to the FLH ($FLH_{AAA1\ mut}$/BLH) resulted in similar effects to those observed for the N-terminally dimerized mutant heterodimers: A $AAA1_{E/Q}$ mutation ($FLH_{AAA1\ E/Q}$/BLH) had a minimal effect on motor velocity, whereas $FLH_{AAA1\ K/A}$/BLH motors suffered a ~3-fold reduction in velocity (Figure 6D). In contrast, introducing the same AAA1 mutations to the BLH (FLH/$BLH_{AAA1\ K/A}$ and FLH/$BLH_{AAA1\ E/Q}$) fully stopped directional motility (Figures 6D and 6E), indicating that the attached linker is solely responsible for force generation. Interestingly, we observed that FLH/$BLH_{AAA1\ K/A}$ motors remained fixed to a single location on the MT, whereas FLH/$BLH_{AAA1\ E/Q}$ motors showed ATP-dependent non-directional diffusive behavior along MTs (Figure 6E). The diffusional motion of FLH/$BLH_{AAA1\ E/Q}$ motors is consistent with reduced MT affinity of the $AAA1_{E/Q}$ monomer in the presence of ATP (Figure 4). Motility was also observed when $AAA3_{K/A}$ and $AAA3_{E/Q}$ mutations were made to the FLH or BLH, with a much stronger effect when present on the BLH. The data present strong evidence that the ATP-dependent linker swing is the force generation mechanism for dynein motility.

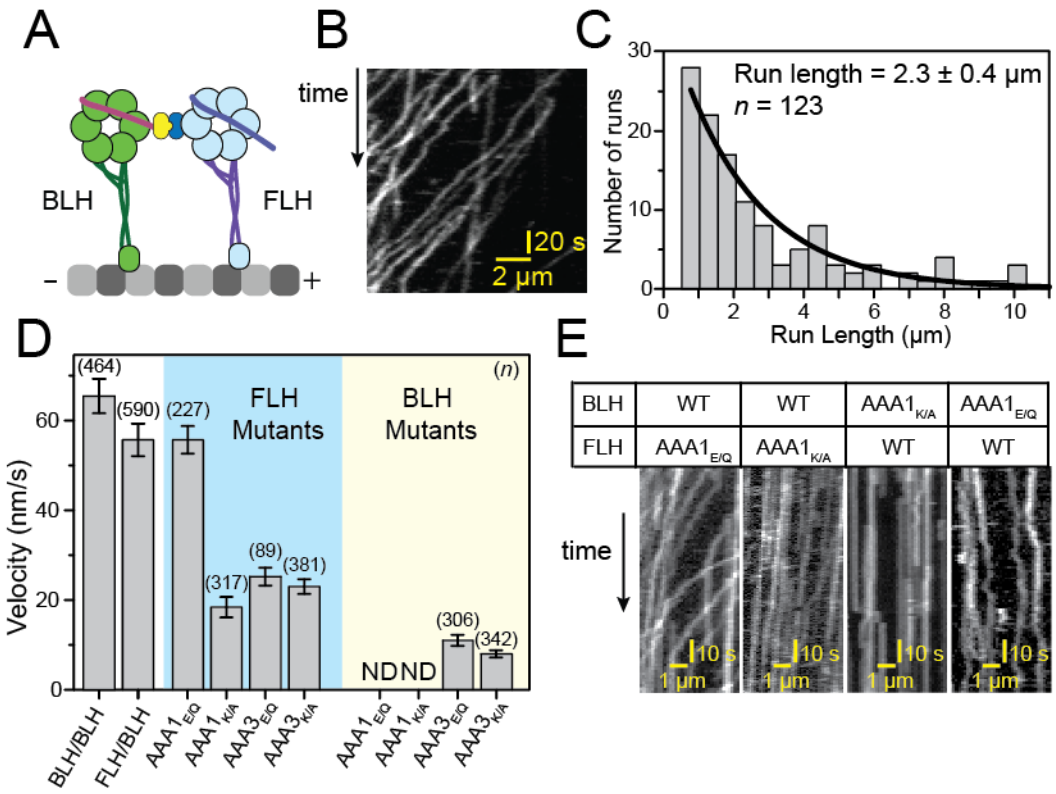

Figure 6. The linker provides force to drive the motility of a dynein dimer. (A) Dimerization of the C-terminal ring of one head to the N-terminal tail of the other results in a dimer of a free-linker head (FLH) and a bound-linker head (BLH). (B) Kymograph showing that the FLH/BLH heterodimer is capable of processive motility. (C) Run length histogram of FLH/BLH at 2 mM ATP, with maximum likelihood fit. (D) The average velocities (± SEM) of FLH/BLH constructs carrying an ATPase mutation in either the AAA1 or AAA3 site in one head (ND: motility not detected). (E) Kymographs of ATPase mutants of the FLH or BLH at 2 mM ATP. The $AAA1_{K/A}$ mutation on BLH abolishes directional motility, whereas $AAA1_{E/Q}$ mutation leads to non-directional diffusion along the MT. The same mutations on FLH do not stop motility, indicating that BLH monomer is responsible for FLH/BLH motility.

Chapter 4. A single ATPase ring can drive dynein processivity

Electron micrographs of axonemal dynein showed that dynein rings are stacked (Nicastro et al., 2006), suggesting that AAA ring-ring interactions may be required for dynein motility. If the two rings in a dimer must coordinate with each other, a dynein heterodimer with a single ATPase ring is not expected to move processively. To test this possibility, we used a "ringless" dynein monomer, in which the AAA ring and the linker are replaced with a monomeric seryl-tRNA synthetase (SRS) (Carter et al., 2008; Gibbons et al., 2005). We tested two strongly bound chimeras, one with a full length dynein coiled coil ($SRS_{85:82}$) and a one quarter length mutant ($SRS_{22:19}$) (Figure 7A). Both constructs showed processive, minus-end directed motion when dimerized with a BLH monomer (Figure 7B). The shorter construct, $SRS_{22:19}$, had a mean velocity of 57.9 ± 13.7 nm/s (mean ± SD) and run length of 0.90 ± 0.16 μm (mean ± 95% confidence interval), while $SRS_{85:82}$ was significantly slower (23.1 ± 8.3 nm/sec) and more processive (1.41 ± 0.25 μm) (Figures 7C and 8). The difference between these two constructs may be due to the geometrical constraints imposed by the altered stalk length. High resolution tracking assays with $SRS_{85:82}$/WT (Figure 7D) showed that $SRS_{85:82}$ had a similar step size distribution to the WT dynein monomer (Figure 7E).

To test whether a ringless head must maintain a high MT affinity for processive motion, we used a $SRS_{89:82}$ construct with an altered coiled-coil registry, which has nearly two orders of magnitude lower MT affinity from $SRS_{85:82}$. $SRS_{89:82}$/BLH was not able to move unidirectionally, and instead diffused along MTs (Figure 9D). The lack of processivity suggests that the inactive MT tether must have a certain minimum MT affinity to allow processive motion of BLH.

We hypothesized that the velocity of the SRS-MTBD/BLH could be increased by decreasing the MT affinity of the SRS-MTBD. Addition of up to 100 mM KCl decreased the dissociation constant (K_d) of the SRS-MTBD from MTs by approximately 30 fold (Figure 9A-C) and increased the velocity of SRS-MTBD/BLH by 50%. Similar results were observed for $FLH_{AAA1\ K/A}$/BLH, but not for FLH/BLH or WT/WT (Figure 9E). Therefore, the increase in motor velocity due to reduced MT affinity is limited to the case of a strongly-bound inactive MT tether attached to an active head.

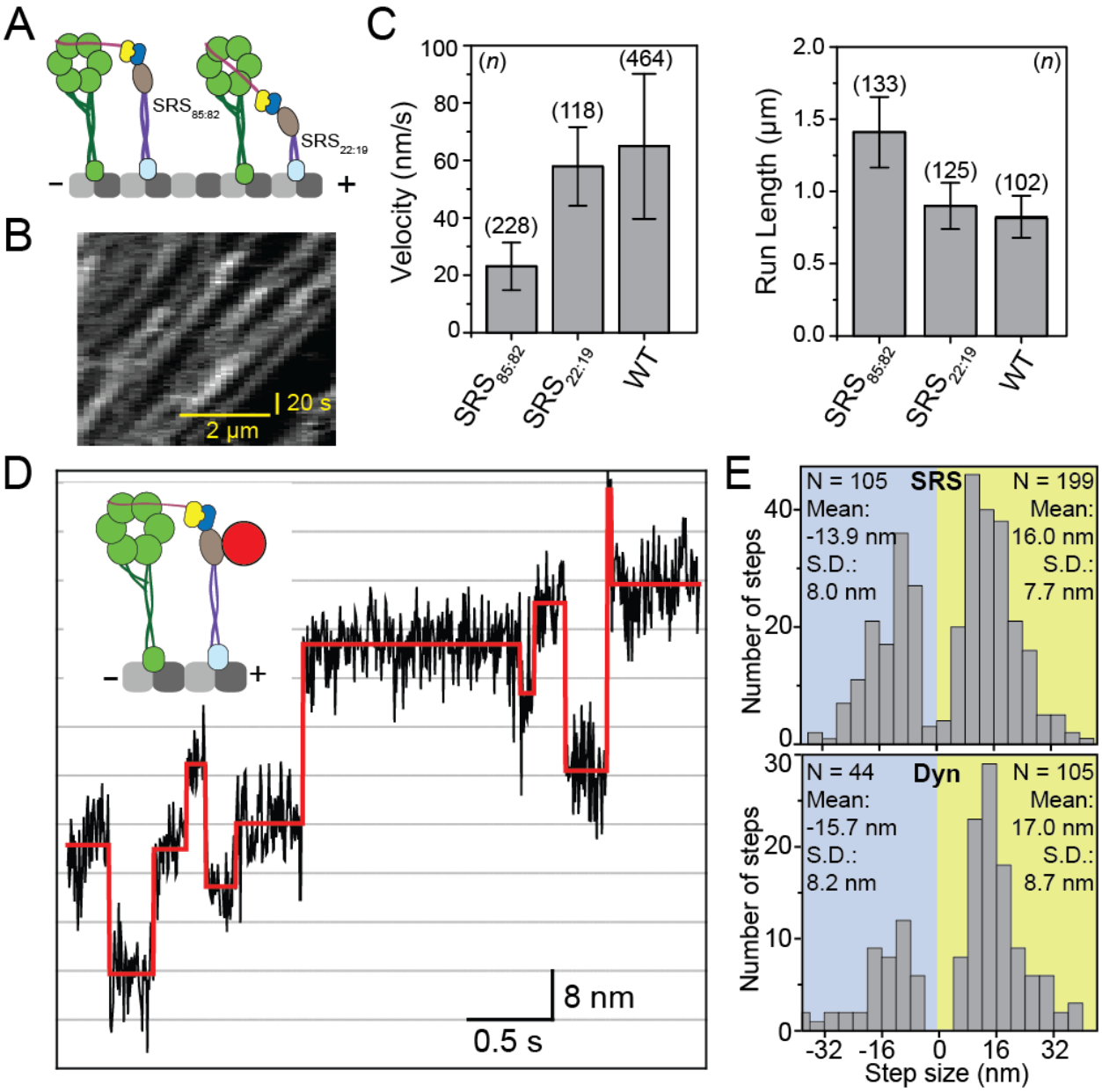

Figure 7. Dynein processivity requires a single motor domain. (A) Possible ring-ring communication between the two heads is abolished by replacing one of the monomers with a SRS-MTBD chimera. (B) A kymograph of $SRS_{85:82}$-MTBD/WT showing that it moves processively along MTs (C) The average velocity (± SD) and run length (± 95% CI) of the SRS-MTBD/WT constructs compared to WT/WT. (D) An example high resolution tracking trace (black) and stepping fit (red) of the $SRS_{85:82}$ head. (E) Histograms of the step sizes for the SRS (upper) and WT (lower) heads.

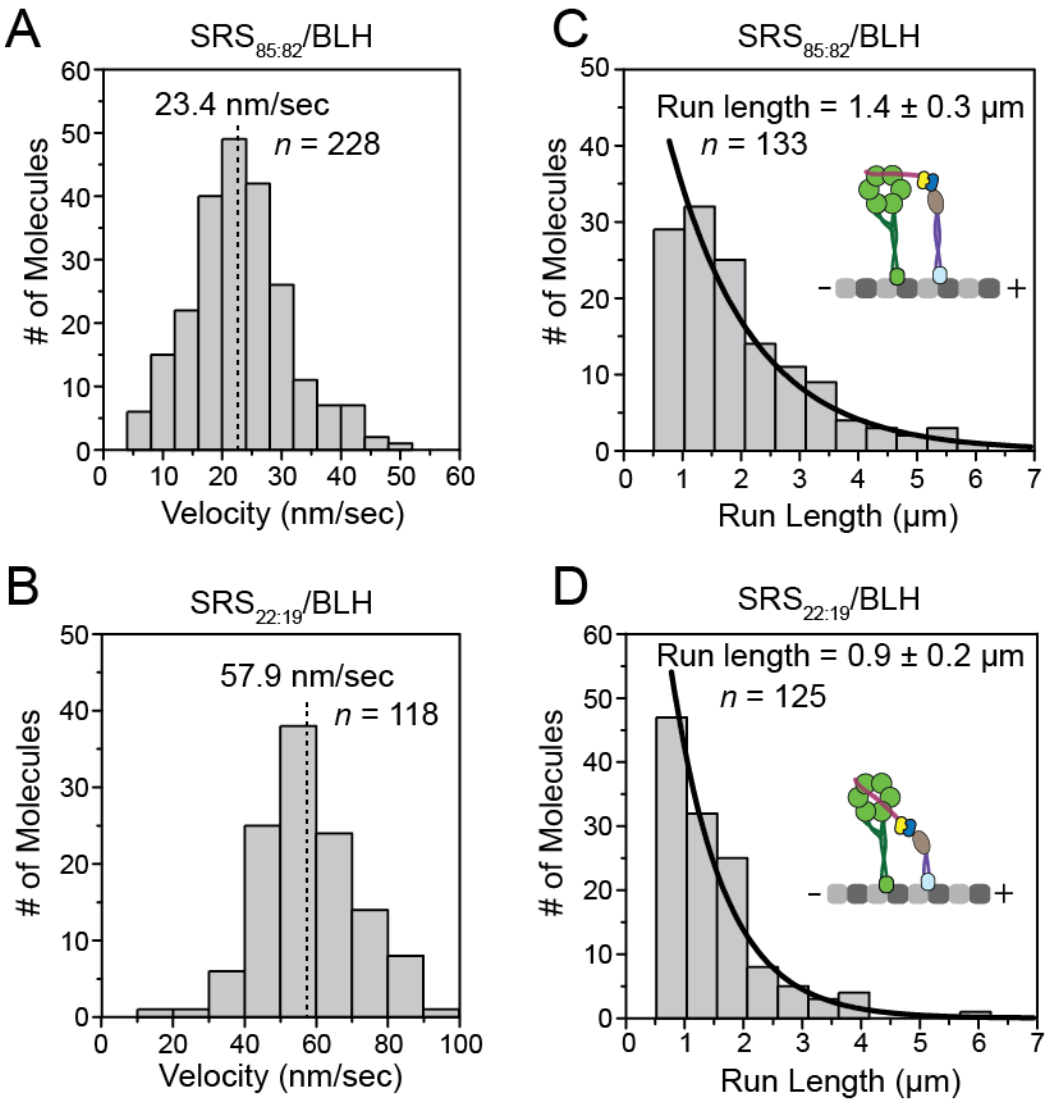

Figure 8. Speed and run length properties of dynein mutants. Velocity (A,B) and run length (C,D) histograms for SRS/BLH motors of different stalk length and same coiled-coil registry. $SRS_{85:82}$/BLH is slower and more processive than $SRS_{22:19}$/BLH.

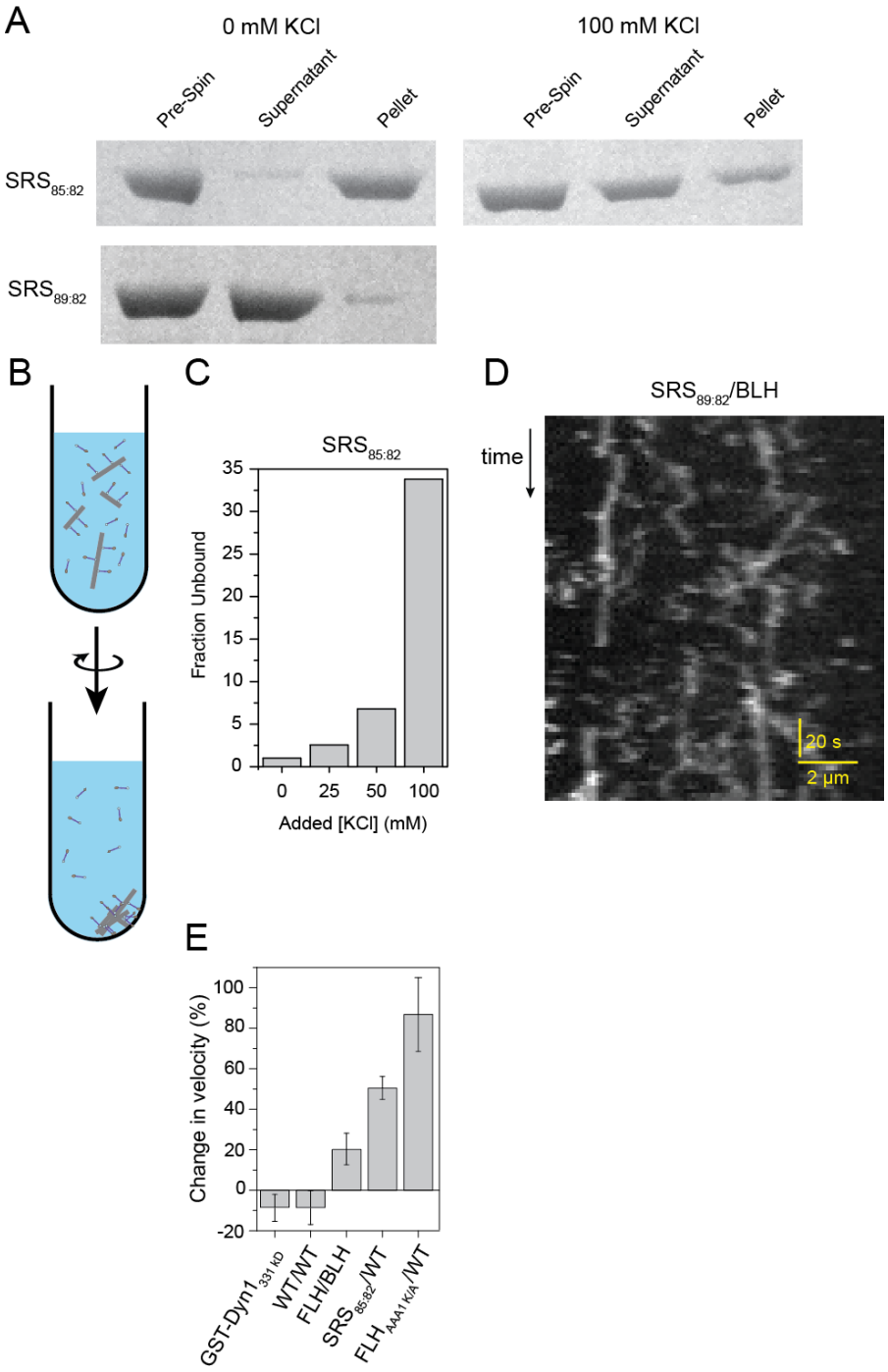

Figure 9. Altered affinity of the SRS chimera for MT in the presence of KCl. (A) SDS-PAGE gel showing the amount of SRS chimera present in assay solution in MT-motor mixture prior to spin (Pre-spin), and in the supernatant and pellet after the spin. (B) Schematic of the MT co-sedimentation assay. (C) Salt-dependent $SRS_{85:82}$ MT-affinity. In two independent experiments the difference in $K_{d\text{-}MT}$ between 0 mM KCl and 100 mM KCl was approximately 30 fold. (D) A representative kymograph showing the non-directional diffusive behavior shown by the $SRS_{89:82}$/BLH motor. (E) Bar graphs show the change in average velocity when 100 mM KCl is added to the assay buffer for the indicated motor (error bars: SD).

Chapter 5. Force-induced release of monomeric dyneins from MTs is strongly asymmetric and dynein's linker domain regulates ATP-dependent MT release

To explore how an inactive head can be dragged forward by an active partner head, we examined the response of dynein monomers to load using an optical trap. Previous motor unbinding force measurements on kinesin were performed by moving a trapped bead unidirectionally at constant velocity along MTs (Uemura and Ishiwata, 2003). These assays do not provide direct determination of MT release at a constant force, because the load increases during a dwell and the unbinding force depends on the bead velocity. To measure the MT-release rate over a wide range of applied forces, we attached dynein monomers to polystyrene beads which were brought in close proximity to a surface immobilized axoneme. The bead was oscillated between two positions 250 nm apart along the MT axis in a square wave pattern at 2 Hz (Figures 10A, B). When a dynein monomer binds to the MT, the bead is unable to return to the center of the trap until the motor releases. During this phase, the trap exerts constant force on the dynein monomer, as a function of the bead-trap separation.

We observed single motor unbinding events at forces ranging from 0.5-12 pN. There was a clear difference in the average time a GFP-Dyn1$_{331kD}$ monomer remained bound to the MT, depending on the direction of the applied load (Figures 10C, 11). When force was applied towards the MT minus end, we observed that the monomers rapidly released from MTs in a force dependent manner (Figure 10C), in agreement with large increase in dynein velocity under forward load (Gennerich et al., 2007). In the no-nucleotide (apo) state, the release rate increased from 5 s^{-1} at 1-2 pN, to 20 s^{-1} at 5-6 pN when dynein is pulled toward the MT minus-end (Figure 10C). In contrast, release towards the plus end is significantly slower (1.5 s^{-1}) and independent of load up to 7 pN, the highest measured stall force of native yeast dynein (Gennerich et al., 2007). This clear directional asymmetry in the MT release rate suggests that the MTBD plays a role in dynein directionality by favoring release of the trailing head. We observed a similar asymmetry in release of the GFP-SRS$_{85:82}$-MTBD chimera, indicating that it is an intrinsic property of dynein's stalk and MTBD, and does not require the AAA+ ring domain (Figure 12A).

To investigate the effect of nucleotide binding to specific AAA sites of the ring on MT affinity, we compared the MT release rate in the presence and absence of ATP. ATP addition was expected to induce an increase in the release rate of dynein (Figure 4) (Imamula et al., 2007). Surprisingly, we observed that 2 mM ATP did not significantly alter the force-dependent release rate of GFP-Dyn1$_{331kD}$, compared to no-nucleotide conditions (Figure 10C).

We hypothesized that the observed ATP independence of the load-induced MT-release rate could be due to pulling dynein through its linker. To test this possibility, we repeated the trapping assay with the bead bound to the C-terminus of a dynein monomer through a short (74 bp) DNA tether (Figures 10A and 10D). In the absence of ATP, we observed similar release rates to those of monomers pulled through the linker domain, implying that DNA attachment does not induce changes in the release rate. Remarkably, the release rate increased several fold upon addition of 2 mM ATP (Figure 10D).

We conclude that in addition to its function as a mechanical element, the linker is involved in coupling the nucleotide and mechanical states of the motor domain. Mutation of the contacts between the linker and the ring affects the ATPase rate of the motor (Kon et al., 2012; Roberts et al., 2009; Schmidt et al., 2012). The load exerted by the trap may disrupt these connections and force the linker to attain a fixed conformation relative to the ring. Our observation that force on the linker influences dynein's ability to release from MT in a nucleotide-dependent manner is consistent with the correlation between MT affinity and linker conformation (Imamula et al., 2007).

We then examined how ATPase mutations in the ring affect the MT release rate of dynein (Figure 12B, C). Similar to a WT monomer pulled through its C-terminus, $AAA1_{E/Q}$ monomers show fast MT release in both the forward and backward directions at 2 mM ATP and slow release in the apo state (Figure 12B). Different from a WT monomer, we did not observe a significant change in $AAA1_{E/Q}$ monomer release rates between forces applied through N- and C-termini (Figure 12B, C). Therefore, $AAA1_{E/Q}$ mutant monomers stay weakly bound to MT regardless of the tension on the linker. Compared to $AAA1_{E/Q}$, $AAA3_{E/Q}$ monomers release at a much slower rate even in the presence of ATP, suggesting that an ATPase deficient AAA3 domain locks the motor in an apo-like state, possibly by affecting the catalytic activity of AAA1.

The results are also consistent with the differences in the velocities of BLH/FLH mutants. We hypothesize that the MT affinity of FLH is the main determinant of FLH/BLH velocity as we observed that the FLH of the fastest BLH/FLH mutants (FLH/BLH and $FLH_{AAA1\ E/Q}$/BLH) show a faster release rate than the FLH of the slower motors (BLH/$FLH_{AAA1\ K/A}$ (an apo motor) and BLH/$FLH_{AAA3\ E/Q}$) (Figure 12B, C).

The observed asymmetry in MT-release could potentially enforce minus-end directionality. According to this idea, reversal of the asymmetry of the MT interface would lead to plus end directed motility. To test this prediction, we replaced the dynein MTBD with the motor domain of human kinesin-1, which favors release towards the plus-end under force (Uemura et al., 2002). We removed the neck-linker and disrupted ATP binding to the kinesin head with a R203K mutation (Thoresen and Gelles, 2008) to prevent any kinesin driven motility. The resulting Dyn-$K322_{R203K}$ chimera had MT release properties opposite to dynein. The release rate increased as a function of force in both directions, with the release towards the plus-end being 20-50% faster than the release towards the minus-end under the same force (Figure 13A).

We next investigated whether the changes to the asymmetry of the MT binding interface reversed dynein directionality. In single-molecule motility experiments, glutathione S-transferase (GST) dimerized Dyn moved toward the MT minus end, with similar motile properties to full length dynein (Reck-Peterson et al., 2006). The GST dimer of Dyn-$K322_{R203K}$ moved processively toward the plus-end at 7 ± 4 nm/s (SD) (Figures 13B, 14B). A construct with an ATPase mutation in the main AAA1 site (Kon et al., 2004) of dynein ($Dyn_{AAA1E/Q}$-$K322_{R203K}$) was immotile, demonstrating that the motility of Dyn-$K322_{R203K}$ is driven exclusively by the ATPase activity of dynein (Figure 13B). Similarly, surface-bound Dyn-$K322_{R203K}$ displayed plus-end directed motility, gliding MTs at 16.2 ± 7.9 nm/s (SD) (Figures 13C, 14A). This was opposite to the directionality of Dyn, which glided MTs at 86.0 ± 10.8 nm/s (SD) (Figures 13C, 14A). High resolution tracking assays revealed that Dyn-$K322_{R203K}$ moved processively by taking 8-32 nm steps in both directions (Figure 13D, E), similar to Dyn. However, it stepped

backward more frequently (45%) than Dyn (~20%) (Reck-Peterson et al., 2006), which may be the result of relatively low asymmetry in MT-release of kinesin (Figure 13E). The average step size was low (1.9 nm) due to frequent backward stepping, which slows down the overall motility of this construct. The results support our hypothesis that asymmetric MT-release under force determines dynein directionality.

In principle, MT-release of a head in a walking dynein dimer could result from interhead tension (Gennerich and Vale, 2009), nucleotide binding to AAA1 (Kon et al., 2004, 2009), or a combination of both effects. In Dyn-K322$_{R203K}$, the MT binding interface is decoupled from the ATPase cycle of the AAA+ ring (Kon et al., 2009), therefore the motor is expected to move by intramolecular tension generated by the powerstroke of the linker (Roberts et al., 2009). To test this possibility, we artificially attached the N-terminus of the linker and the tip of the stalk of a dynein monomer to two artificial handles terminating with the dynein MTBD (Carter et al., 2008) (Figure 15). The construct moved towards the MT minus-end at 12 ± 1 nm/s (SEM), suggesting that asymmetric MT-release in combination with tension generated by the motor domains is sufficient to drive minus-end directed motility.

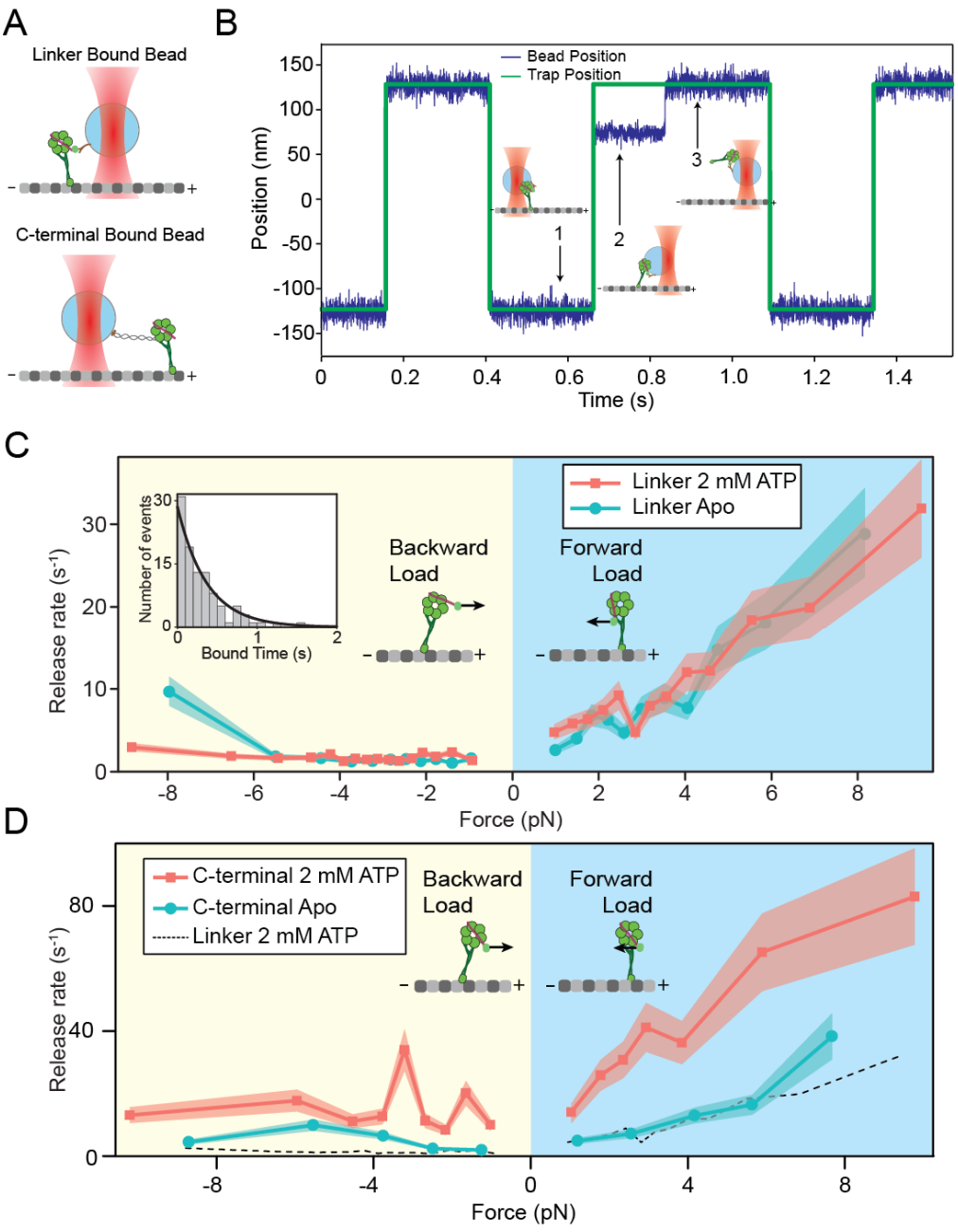

Figure 10. Tension on the linker inhibits nucleotide-dependent release of dynein from MTs. (A) Dynein monomers are attached to a polystyrene bead either through the N-terminus of the linker via a GFP-antibody linkage, or through the C-terminus of the ring via a 74 bp long DNA tether (not to scale). (B) A representative trace showing bead position (blue) and trap position (green). (C) Force-dependent release rates of dynein monomers when the trapped bead is attached to the N-terminal linker domain. The distribution of the forward and backward release rates are unaffected by the presence (red, n = 3003) and absence (blue, n = 2335) of ATP. Shaded regions indicate 95% confidence intervals. Inset: A representative example of the distribution of measured MT bound times within a bin, with maximum likelihood fit. (D) Force-dependent release rates when dynein is pulled through the C-terminus. The rate is similar to the N-terminal attachment case (dotted black line) in the absence of ATP (blue, n = 1105), but increases several fold in the presence of 2 mM ATP (red, n = 1652).

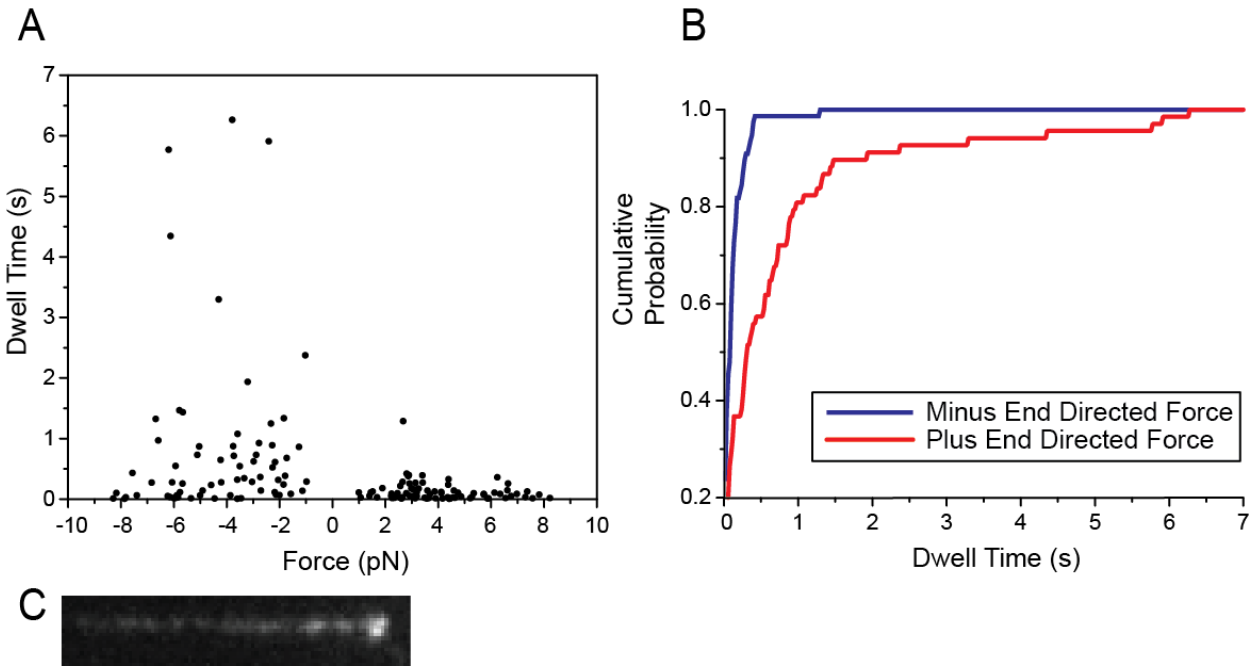

Figure 11. Dynein monomer-MT release rates are asymmetric depending on direction of applied force. (A) Scatter plot of applied force and dwell time for both plus- (negative values) and minus-end (positive values) directed force for a Dyn monomer. All of the events (n = 145) shown were scored on a single axoneme. (B) Cumulative distribution functions for dwell time in each direction for all the events scored on a single axoneme for a Dyn monomer. MT release was 3-10 fold faster when force is applied in one direction than the other. (C) An axoneme whose minus end is decorated with Alexa488-labeled dynein motors.

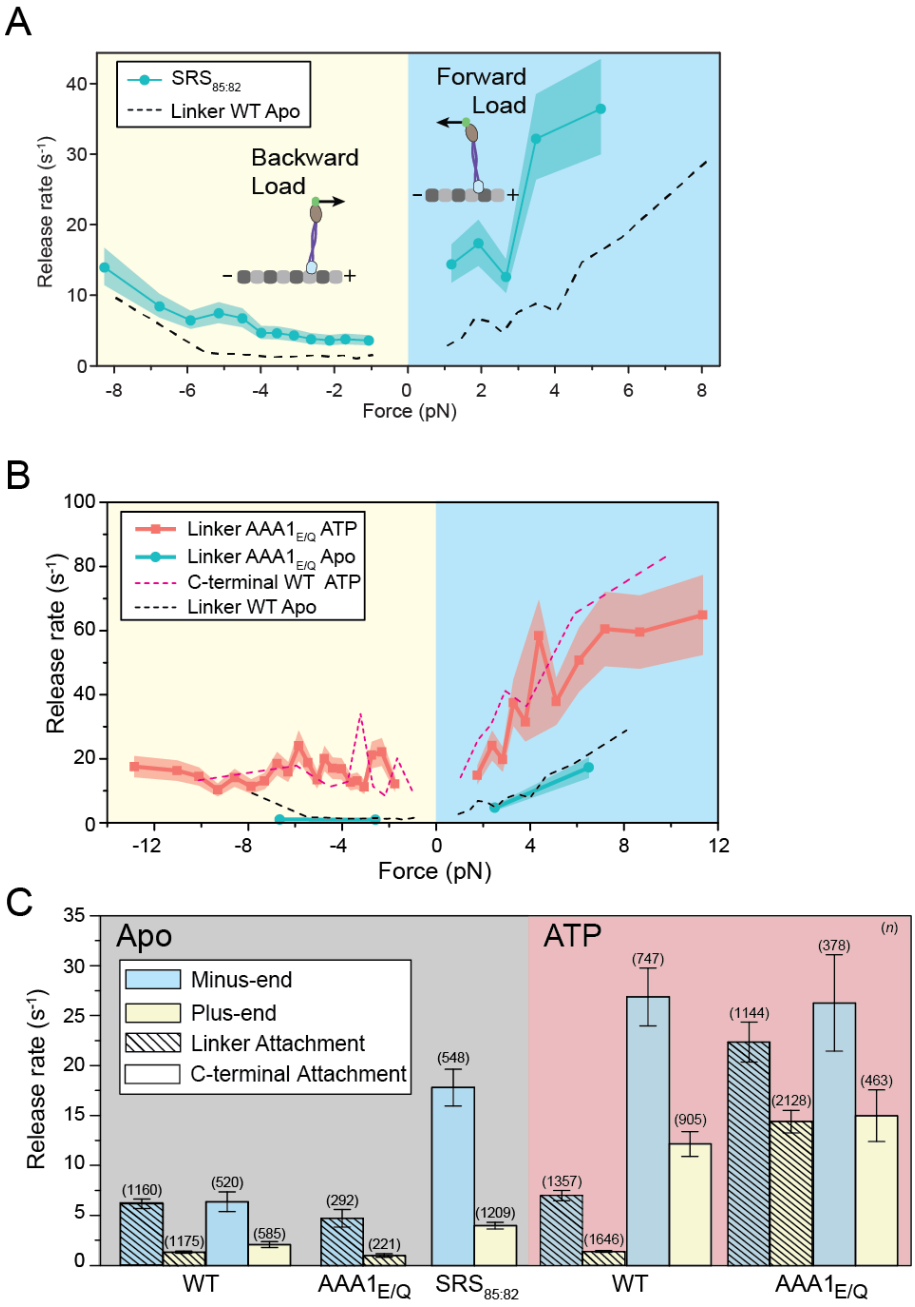

Figure 12. The force dependent MT-release rates of the dynein MTBD and of ATPase mutants. (A) $SRS_{85:82}$-GFP, which contains the dynein MTBD from mouse, shows a tendency to release towards the minus end at a faster rate to a yeast WT dynein monomer pulled through its linker in the absence of ATP (dotted line). Shaded regions show 95% confidence intervals, n = 1757. The data indicate that the asymmetry in release rate is an intrinsic property of dynein's stalk and MTBD, not the AAA+ ring. (B) The force dependent release rate of an $AAA1_{E/Q}$ mutant pulled through the N-terminus in the presence (red, n = 3272) and absence (blue, n = 513) of ATP. Rates of the C-terminal attached WT head with ATP (magenta dotted line) and N-terminal attached WT without nucleotide (black dotted line) are shown for comparison. $AAA1_{E/Q}$ releases at similar rates to WT when pulled through the linker in the apo state. In contrast to WT, $AAA1_{E/Q}$ shows fast nucleotide dependent release when pulled through the linker at 2 mM ATP. (C) The average release rates of dynein mutants under 1-3 pN of load either toward the minus (blue) or plus (yellow) end of MTs (± 95% CI). Hashed bars indicate N-terminal attachment, solid bars indicate C-terminal attachment.

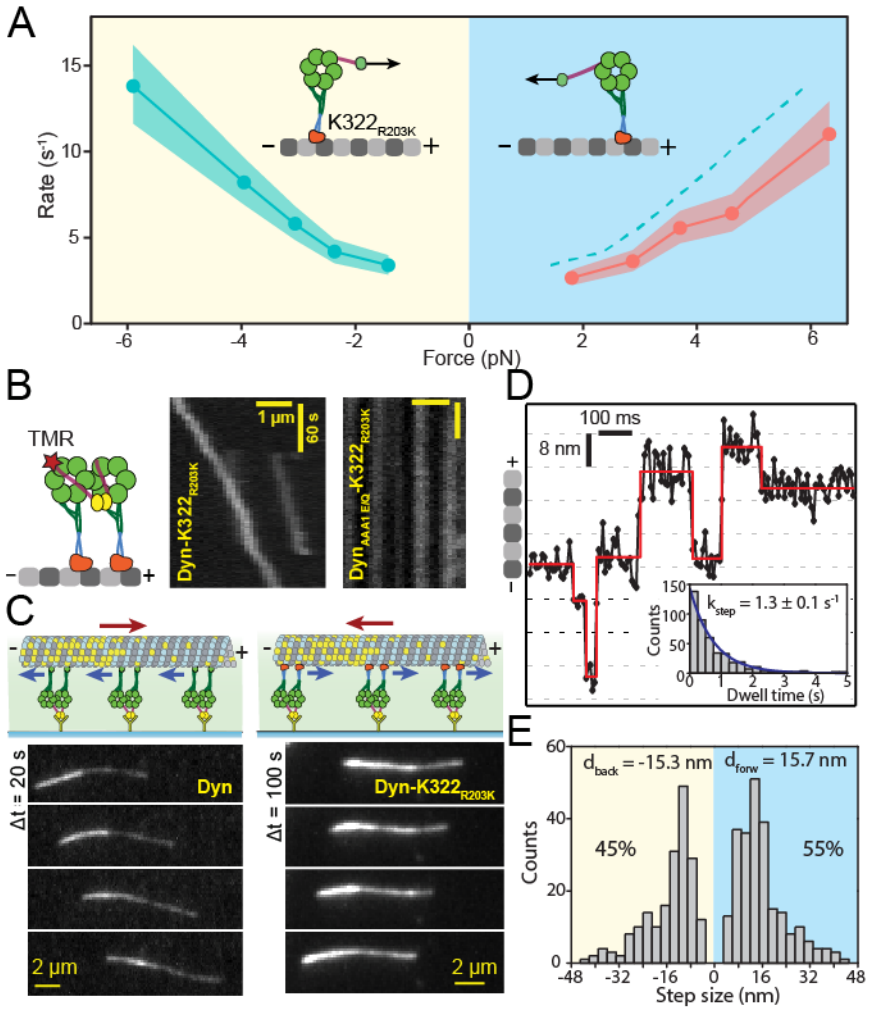

Figure 13. Replacing the dynein MTBD with a kinesin motor domain reverses both the asymmetry of MT release and dynein directionality. (A) The MT release rate of a Dyn-K322$_{R203K}$ monomer increases with force in both forward and backward directions. Release towards the plus end is faster than that towards the minus end through a wide range of applied forces. The dotted line on left represents the MT release rate towards the plus-end for comparison. Shaded regions indicate 95% confidence intervals. (B) Kymographs representing the single-molecule motility of chimeric constructs with ATPase mutations. Dyn-K322$_{R203K}$ moves towards the plus end and Dyn$_{AAA1E/Q}$-K322$_{R203K}$ remained immotile, showing that plus-end directed motility of Dyn-K322$_{R203K}$ is powered by the dynein motor domain. (C) (Top) Schematic representing MT gliding assay with a polarity marked MTs (bright minus end). (Left) Dyn glides MTs with the plus end in the lead (red arrow), in agreement with its minus-end directed motility (blue arrows), while Dyn-K322$_{R203K}$ glides the MTs in opposite direction (Right). (D) Stepping trace of Dyn-K322$_{R203K}$. (Insert) The stepping rate of Dyn-K322$_{R203K}$ (1.3 s^{-1}) was 5-fold lower than Dyn[10]. (E) Step size analysis of Dyn-K322$_{R203K}$ shows highly frequent (45%) backward steps (n = 435 steps).

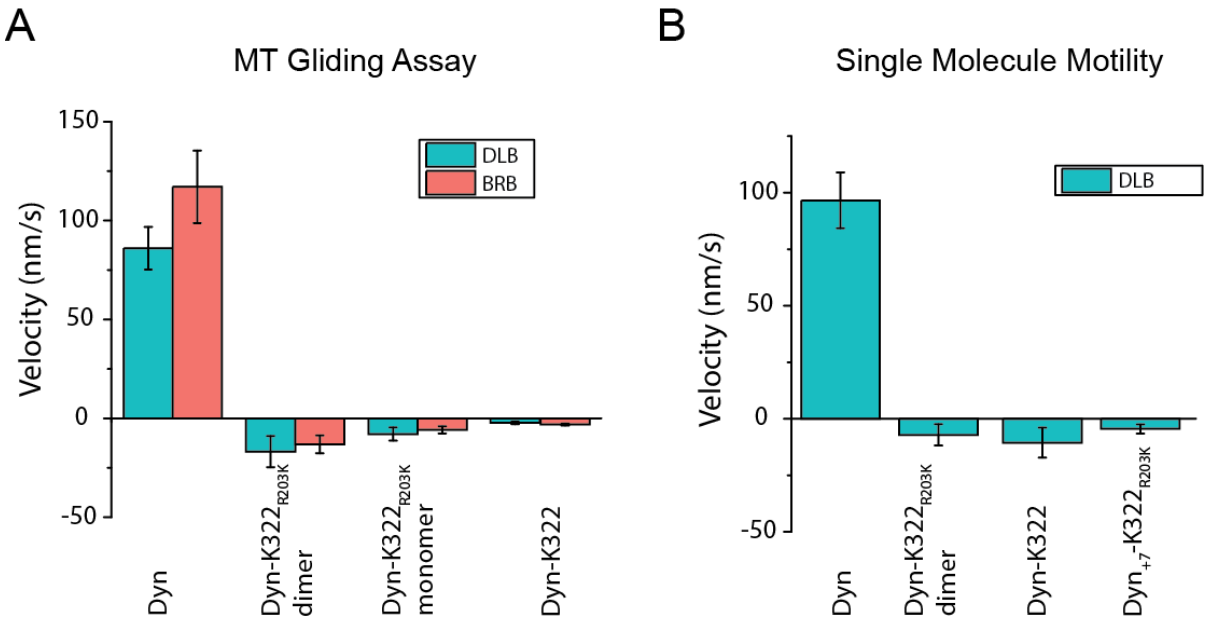

Figure 14. The velocities of wild-type and chimeric dynein constructs in MT gliding and single molecule motility assays. (A) Gliding assays were performed either in dynein loading buffer (DLB), or kinesin assay buffer (BRB80). (B) Single molecule motility assays were performed in DLB. Exchanging the dynein MTBD with the kinesin motor resulted in reverse directionality in all constructs tested under multiple assay and buffer conditions. Notably, reversing the relative orientation of the kinesin motor with respect to the dynein motor and its priming stroke by adding an extra heptad repeat to the stalk region of the dynein motor (Dyn_{+7}-$K322_{R203K}$) still resulted in plus-end directed motility. Error bars represent S.D. (Gliding: $n_{\text{Dyn-DLB}} = 89$, $n_{\text{Dyn-BRB80}} = 47$, $n_{\text{Dyn-K322R203K-DLB}} = 50$, $n_{\text{Dyn-K322R203K-BRB80}} = 118$, $n_{\text{Dyn-K322R203K-monomer-DLB}} = 49$, $n_{\text{Dyn-K322R203K-monomer-BRB80}} = 40$, $n_{\text{Dyn-K322-DLB}} = 97$; Single molecule: $n_{\text{Dyn}} = 130$, $n_{\text{Dyn-K322R203K}} = 44$, $n_{\text{Dyn-K322}} = 41$, $n_{\text{Dyn-+7-K322R203K}} = 35$).

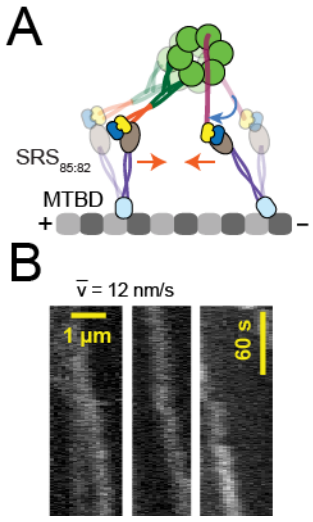

Figure 15. Tension created by the dynein motor domain is sufficient to drive motility. (A) The engineering of a "compression motor" that generates tension (red arrows) between two MT attachment sites. A dynein monomer lacking the MTBD was coupled to two handles terminating with MTBD at the tip of the stalk and the N-terminus of the linker (left). (B) Kymograph representing the minus-end directed processive motility of the compression motor and the mean velocity

Chapter 6. A model for dynein motility

We combined our experimental results and developed a quantitative model for dynein motility in which a head can release from the MT either through ATP binding or by tension (Figure 16A). At low separations, the heads are fully uncoordinated and either head binds ATP and takes a step with a rate of 8 s^{-1} (Reck-Peterson et al., 2006). While one of the heads takes a step, the other head serves as a tether to prevent release of the motor from MT. At high interhead separations, tension on the linkers prohibits ATP induced release of a head and prevents this mode of stepping (Figure 16A). In this case, a head releases from MTs under tension and relieves the tension by stepping towards the tethered head. Release rates under tension were inferred from fits to the optical trap data (Figures 12 and 17).

We used reported step size (DeWitt et al., 2012; Qiu et al., 2012) and ATPase rates (Cho et al., 2008; Reck-Peterson et al., 2006), as well as our optical trapping data, to test if our model could accurately capture the behavior observed in native and mutant forms of yeast dynein. Monte Carlo simulations were used to generate stepping traces of a WT/WT dynein dimer. Simulated traces (Figure 16B) reproduced uncoordinated stepping patterns, with a significant fraction (33%) of steps in the backward direction. At high interhead separations, the majority of the steps were taken by the rear head, as observed experimentally (Figure 16C) (DeWitt et al., 2012; Qiu et al., 2012). The model estimated that the overall stepping rate per head is 7 s^{-1}, in agreement with the MT stimulated ATPase rates and the tension-induced stepping pathway constitutes a significant fraction (32%) of dynein stepping motion.

We also tested whether our model could reproduce the observed response of dynein motility to ATPase mutations and altered dimerization geometry. In simulations of these mutants, C- and N-terminal trapping data were used to calculate the force induced release rates of FLH and BLH, respectively (Figure 17). Different from WT dynein, the FLH and $AAA1_{E/Q}$ mutant heads in the model do not undergo a powerstroke, but do release from the MT due to bound ATP (Figure 12). The velocities of simulated motors were in strong agreement with the measured velocities of mutant heterodimers (Figure 16D). Although dynein's stepping mechanism may be more complex than the model depicted here, the results show that the tension-induced gating mechanism explains the stepping properties of dynein motility.

The stiffness of the linkage between the dynein heads remains unknown; therefore the tension between the heads cannot be directly inferred from the interhead separation. We tested a wide range of stiffness values (Figure 18) and found that the stiffness of 1 pN per 12 nm extension of the linker agreed most closely with the experimental results (Figures 16D and 18). Because most (83%) dwells have an interhead separation of less than 36 nm, we estimate that dynein heads experience up to 3 pN tension, equivalent to maximal force production of a single dynein motor (manuscript in preparation). See Methods for a detailed description of the parameters used in the model.

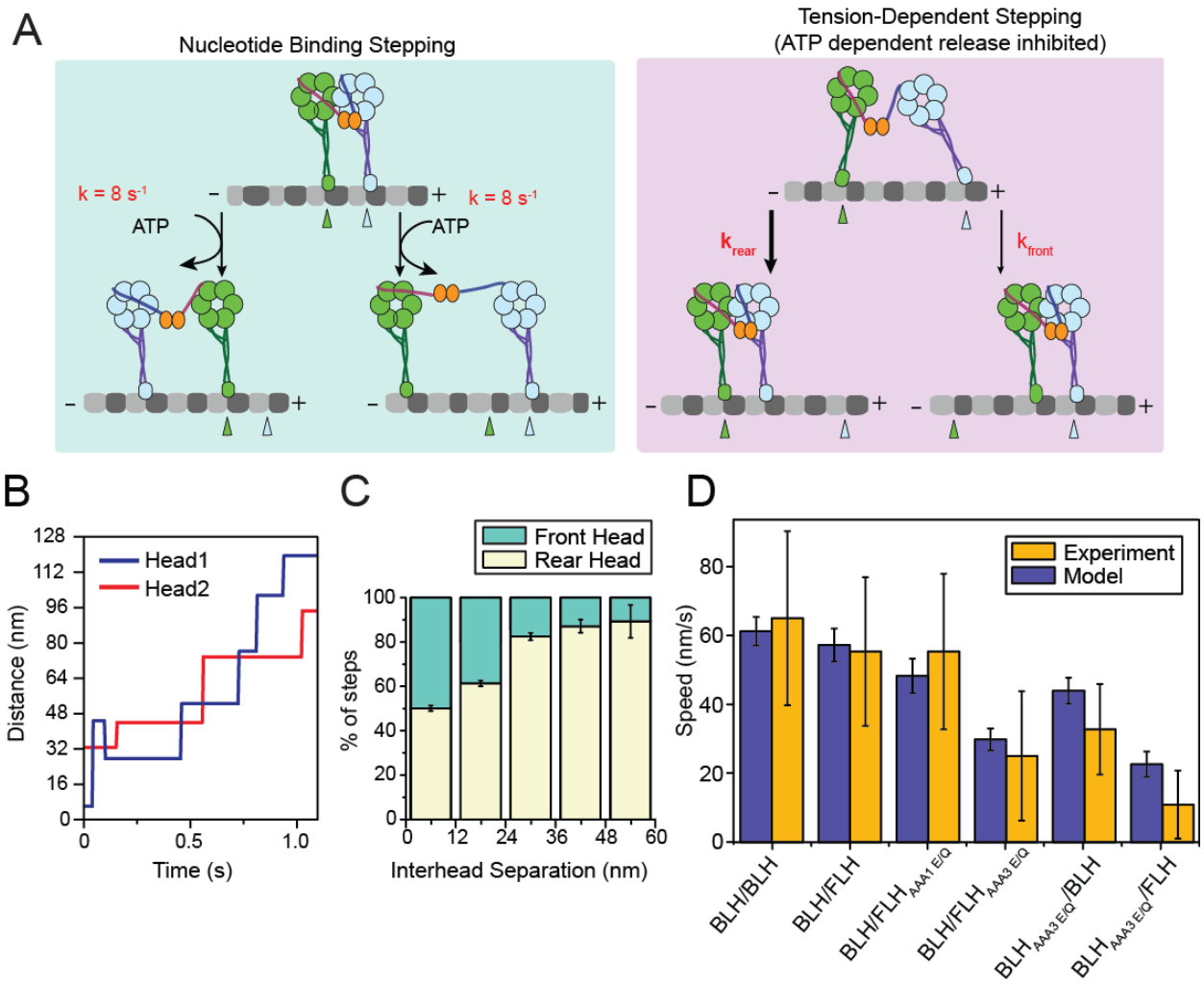

Figure 16. A model for dynein motility. (A) Two proposed mechanisms of dynein stepping. (Left) When the heads are close to each other, either head can release the MT and step forward upon binding ATP. (Right) When the heads are far apart, tension on the linker prevents ATP-dependent MT release, and the asymmetry of the release rates under tension favors the trailing head to take a step. (B) A representative Monte-Carlo simulation of dynein motility shows stepping of the two head domains (blue and red). (C) The trailing head is more likely to take a step in simulated traces as the interhead separation increases. The data shown is the average of 200 simulations (± SD). (D) The average velocity of 200 100 s simulated traces (± SD) agrees well with measured velocities for various dynein mutants (± SD).

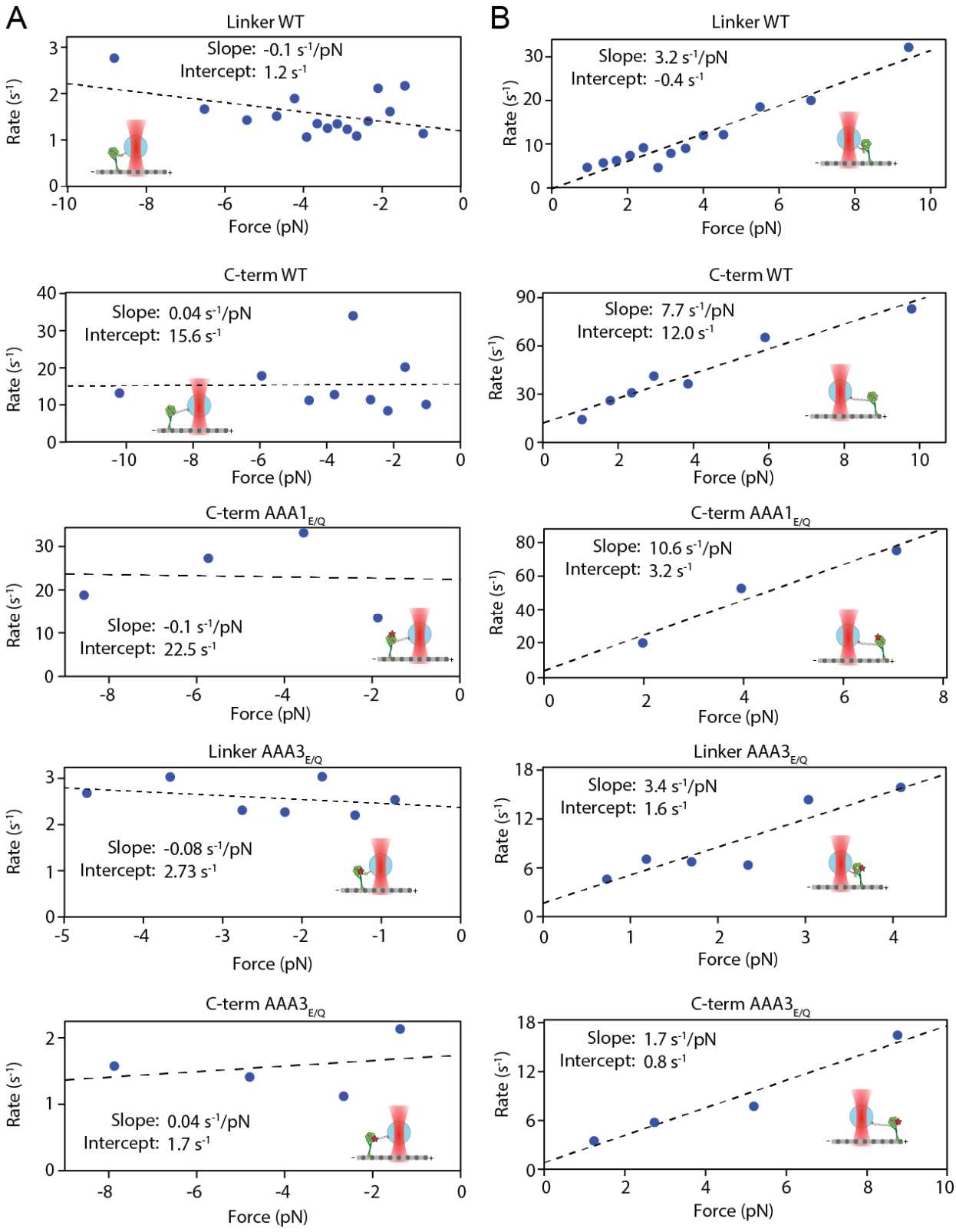

Figure 17. Linear fits to optical trap data used in modeling dynein stepping. Fits and their values are shown for the indicated mutants for plus-end directed (A) and minus-end directed (B) force.

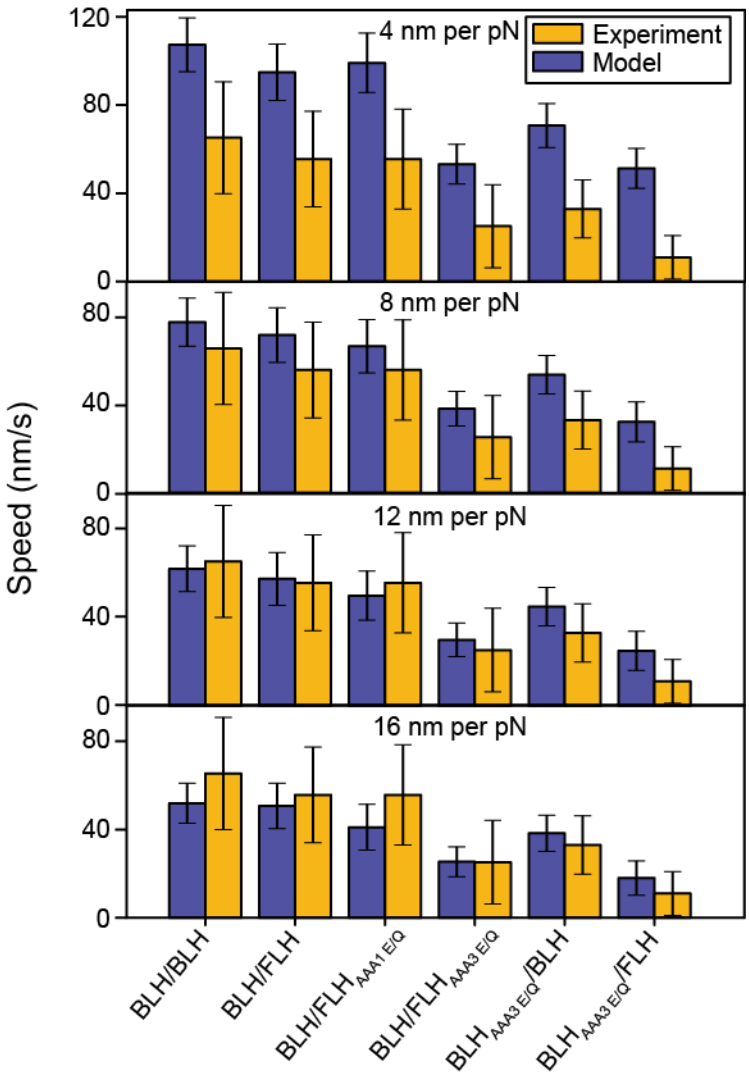

Figure 18. The stiffness of the linkage between dynein monomers does not affect the overall trend of the model. Simulations were run with the indicated stiffness between motors (12 nm per pN was used in figure 6). The mean and standard deviation of 200 20 s simulations for each mutant is shown for each stiffness, along with the experimental results.

Chapter 7. Discussion

Our single molecule experiments on engineered dynein mutants have revealed the minimal requirements of dynein processivity, force generation and directionality. We found that increasing the flexibility or altering the dimerization geometry of the linkers do not abolish processivity. A single monomer is able to drive processive motility at 82% of the native dynein velocity even with its partner AAA+ motor replaced by an inert protein. Optical trapping studies on monomeric dyneins showed that the MT-binding interface prefers to release under force towards the MT minus-end, providing strong bias for the unidirectional motion of dynein. Interestingly, exerting forward and backward forces through the linker domain disrupts nucleotide-dependent MT release, suggesting that the conformation of the linker is coupled to nucleotide-dependent release from MTs. The implications of these findings for dynein's stepping mechanism are discussed below.

Defining a Minimal Processive Dynein Motor

Previous studies on recombinant cytoplasmic dynein have shown that individual dynein motor domains are incapable of processive movement and dimerization restores processivity (Reck-Peterson et al., 2006), contrary to reported processive motility of single headed axonemal dynein c motors (Sakakibara et al., 1999). A N-terminal truncation of the tail domain to aa 1390 (Dyn_{314kD}, similar to 365 kDa for *Dictyostelium* dynein (Nishiura et al., 2004)) does not substantially affect motility, but further deletion of 26 amino acids causes a complete loss of motility (Reck-Peterson et al., 2006). However, it remained unclear whether dynein motility specifically requires both monomers to be catalytically active, dimerized through their N-termini, communicating their nucleotide cycles and mechanically coupling their stepping motions with each other.

Our experiments have precisely defined the mechano-chemical requirements for dynein processivity. Processivity does not require two catalytically-active motor domains. Altering the ATPase activity of a single monomer in dynein heterodimers revealed a strikingly different phenotype from identical mutations to homodimeric constructs (Cho et al., 2008; Kon et al., 2004). A hydrolysis deficient AAA1 mutant heterodimer moved at near WT velocities. These results differ significantly from similar measurements on kinesin motility. A kinesin heterodimer carrying a single ATP hydrolysis (Thoresen and Gelles, 2008) or ATP binding (Kaseda et al., 2003) mutation moves processively, but the velocity was 10 - 20 fold slower than native kinesin. In dynein, a single force-generating head is able to drive motility nearly as fast as if both heads retained full ATPase activity, provided its inactive partner has moderate affinity for the MT. We also showed that dimerization through the tail domain is not essential for processive motility, inconsistent with the proposed role of the tail domain for interhead coordination in dynein motility (Ori-McKenney et al., 2010).

Dynein's unique domain architecture has made it possible to isolate the MT-binding interface from its catalytic core. We showed that the entire AAA ring and linker domains of FLH can be replaced with an inert protein retaining the MTBD and part of the stalk. Therefore, dynein motility does not require both AAA+ ring domains, and the partner motor does not need to cycle between weakly and tightly MT-bound states. These results raise the possibility that synthetic

processive motors may be engineered from a single polypeptide containing one catalytic ring domain and two MT attachment sites in future studies. Our ringless dynein heterodimer also excludes direct mechanical or allosteric interactions between the two AAA+ rings as a required mechanism for processivity or force generation.

We present conclusive evidence that tight communication between the two heads is not required for processivity. Established views on motor processivity suggest that a motor would dissociate from its track after a few steps in the absence of gating (reviewed in Block, 2007). In the absence of interhead communication, dynein processivity could arise if the duty ratio of a head is sufficiently high (~0.9) to allow the motor to take 100 steps (the average run length is ~1 μm and the average step size is ~10 nm) before dissociation (DeWitt et al., 2012). The duty ratio of *Dictyostelium* dynein was estimated to be a minimum of 0.6 by the filament gliding assays (Shima et al., 2006b). Here we showed that the processivity of engineered dynein heterodimers is correlated with the MT affinity of the mutant head (Figures 4 and 5C). This finding is consistent with dynein processivity arising from a high duty ratio, and not gating of the heads.

The role of the linker in dynein stepping

In the apo and ADP states, the linker lays across the ring, spanning from AAA1 to AAA4 (Kon et al., 2012) or AAA5 (Schmidt et al., 2012). In the ADP.P_i state, the linker position becomes variable, with its N-terminus occupying positions from AAA5 to AAA2 (Roberts et al., 2009). This "linker swing" is proposed to power dynein movement. Consistent with this hypothesis, dynein monomers tethered by their C-terminal ring are either unable to glide MTs (Reck-Peterson et al., 2006) or glide MTs with a hundred-fold reduced velocity (Shima et al., 2006a). Engineering of a processive dynein dimer with mechanically distinct monomers allowed us to investigate in depth the function of the linker in dynein's stepping mechanism. By selectively disrupting the linker swing in FLH and BLH mutants, we present strong evidence that the linker powers dynein motility and its N-terminus must be tethered to a second MT binding site to generate an efficient powerstroke.

Unlike kinesin, dynein mutants bearing a flexible insert in the linker region were able to move processively at near WT velocity. Processive movement does not require a rigid body attachment between monomers, consistent with dynein's ability to attain a wide variety of interhead orientations during processive motility (DeWitt et al., 2012). Because dynein mutants with flexible inserts conserve directionality, we propose that a detached head is not oriented towards the MT minus end by its attached partner.

Our optical trapping assay indicates that force on the linker regulates dynein's MT affinity. Reducing the linker length (Reck-Peterson et al., 2006) or mutating the residues on AAA5 that make contact with the linker almost eliminate MT stimulated ATPase activity (Schmidt et al., 2012), indicating that contacts between the linker and the ring are essential for ATPase activity. Forces exerted on the linker may disrupt these contacts and trap the nucleotide cycle. This inhibited state has similar MT release rates to the apo state, suggesting that the linker may be required to reorient around the ring to allow ATP binding or the release of hydrolysis products from AAA1.

It is also possible that the linker directly couples MT affinity to the ATP hydrolysis cycle. In this case, dynein monomers are expected to show a defect in release when pulled through the linker independent of any ATPase mutations in the ring. However, we observed that $AAA1_{E/Q}$ monomers have different release rates from WT when force is applied to the linker domain. A coiled-coil segment extending from AAA5 (Carter et al., 2011; Kon et al., 2011) was proposed to participate in long range communication between the catalytic sites and the MTBD. Since the linker runs across the opposite side of the ring (Kon et al., 2012; Schmidt et al., 2012), it is unlikely that the linker orientation directly affects MT affinity. Instead, we propose that linker configuration is directly coupled to the catalytic activity of the ring, and forcing the linker to a fixed conformation indirectly affects the MT affinity.

The Mechanism of Dynein Directionality

Several theories have emerged to explain the minus end directionality of dynein. Powerstroke models suggest that the priming stroke of the linker points the MTBD towards the minus-end (Burgess et al., 2003). The linker swings parallel to the MT long axis (Roberts et al., 2009), presenting further evidence that the reorientation of the linker relative to the ring determines dynein directionality. Consistent with this idea, changing the orientation of the power stroke of myosin V lever arm (Bryant et al., 2007) and the neck-linker docking of kinesin (Sablin et al., 1998) reversed motor directionality. However, reversing the orientation of the ring with respect to MT did not alter dynein directionality (Carter et al., 2008), suggesting that the directional preference of dynein is specified by an element outside of the catalytic domain.

The directionality of dynein motility can be manipulated by external forces both in the presence and absence of ATP, with strong preference to move towards the minus end (Gennerich et al., 2007). However, the force-response of a single MTBD remained unclear, because load could be sensed by both MTBDs when dimers are pulled by the trap. Our optical trap measurements on monomeric dynein have measured a strong asymmetry in the MT-binding interface. The release towards the plus end is slow and load-independent, whereas the release towards the minus-end is faster and increases under assisting load. The MT-release rates of WT dynein monomers are compatible with the velocity of force-induced bidirectional motility of dimeric dynein (Gennerich et al., 2007), and also explain the differences between the velocities of dynein mutants carrying distinct ATPase mutations (Figure 5C). We propose that a dynein head can release from MTs in both nucleotide and tension dependent manners (Figure 16A). While dynein is able to move processively without a rigid connection between the two heads, the linker domains can generate tension between two monomers at large interhead separations. Tension would thus cause the rear head to preferentially release from MT in a nucleotide-independent manner.

We propose that the preferential binding and release properties of the dynein MTBD, coupled with ATP-dependent conformational changes of the linker, break the symmetry of diffusion and provide minus-end directionality (Figure 16A). The tension-induced release mechanism we describe is likely to predominate at larger interhead separations (Figure 16A). Rearward tension on the leading head results in a slow (~1.5 s^{-1}) release rate, while the trailing head, being under forward tension, releases at a much faster rate. Consistent with this model, stepping studies showed that the trailing head steps more frequently than the leading head at large interhead separations (DeWitt et al., 2012; Qiu et al., 2012).

When the heads are close together with no or little tension between them, either head releases from the MT upon ATP binding. The released head searches for tubulin attachment site by diffusion and preferentially binds the MT when the stalk is tilted toward the plus end, as suggested by electron micrographs of MT-bound dynein (Carter et al., 2008; Oda et al., 2007; Redwine et al., 2012). As a result, the released head more likely rebinds the MT at a location towards the minus end from its partner head. The priming stroke may increase the distance between the tail and the MTBD of the released head, allowing access to more tubulin sites via diffusion. Consistent with earlier protein engineering approaches in *S. cerevisiae* dynein(Carter et al., 2008), reversing the priming stroke in a Dyn-K322$_{R203K}$ construct did not affect directionality (Figure 14).

In this work, we successfully engineered a chimeric motor that uses the dynein motor ATPase to move towards the plus end, demonstrating the principle that underlies dynein directionality. We observed similar release properties of the mouse dynein MTBD (Figure 12), suggesting that the intrinsic asymmetry of the MTBD is well conserved in eukaryotes. The ability to remain attached to MTs under high backward forces may be essential for multiple dyneins to transport large intracellular cargos under high tension (Rai et al., 2013), and to anchor MTs to the cell cortex during cell division (Ananthanarayanan et al., 2013). Mammalian dyneins, which stall at lower forces (Mallik et al., 2004; McKenney et al., 2010), were shown to reverse directionality by the dynactin complex (Ross et al., 2006), suggesting that the asymmetry in dynein-MT interactions can be modulated by external factors. The method we developed will be applicable to the dynein/dynactin complex and other cytoskeleton anchoring proteins to provide quantitative assessment of their release properties under tension.

Methods

Construct Design and Yeast Cloning

An N-terminal truncated *S. cerevisiae* cytoplasmic dynein gene (*DYN1*) encoding amino acids 1219-4093 (predicted molecular weight 331 kD, referred to as Dyn) was used as a template for mutagenesis (Reck-Peterson et al., 2006). Dyn was artificially dimerized through an N-terminal GST tag (GST-Dyn). An N-terminal GFP fusion protein of GST-Dyn (GFP-GST-Dyn) has been shown to move at similar velocity and processivity to that of native yeast dynein (Reck-Peterson et al., 2006).

Strains CY29, CY40 and CY134 (see Table 1) were generated as described in (Carter et al., 2008). The chimeric dynein/kinesin constructs in the case of yeast strains CY151 and CY412 consisted of amino-acid residues Q236 – T284 of colicin Ia, amino-acid residues L4 – A322 of human conventional kinesin, a GS-linker and amino-acid residues R384 – I432 of colicin Ia and were integrated in the genomic copy of the dynein motor domain (Dyn_{331kD}) between L3034 and I3293. Dynein driven motility was disrupted by introducing the AAA1 E/Q mutation E1849Q (Cho et al., 2008). The ATPase activity of human kinesin-1 was disrupted by introducing the R203K mutation, which is equivalent to the well-studied R210K mutation in Drosophila kinesin (Klumpp et al., 2003). The constructs in the case of yeast strains CY379, CY384 and CY412 were the same except for the R203K point mutation in the human conventional kinesin region. CY413 was based on CY379, but in this case the colicin-kinesin-colicin region was integrated in the genomic copy of the dynein motor between Q3083 and K3244. All chimeric dynein/kinesin constructs were generated by PCR-stitching from plasmids containing S. cerevisiae cytoplasmic dynein, the coiled-coil region of colicin Ia and human conventional kinesin.

To generate the corresponding yeast strains, PCR-products were transformed into CY29 (CY399), CY40 (CY379, CY412 & CY413) or CY134 (CY151 & CY384). The dynein used in the compression motor experiment was generated by inserting the same colicin Ia and GS-spacers to the same location in dynein as the kinesin insert constructs, with the kinesin domain replaced by an FRB heterodimerization domain, into VY209, a strain with an N-terminal FRB domain.

Heterodimeric dynein constructs were obtained by replacing the GST tag of GST-Dyn with an FRB tag on one monomer (FRB-Dyn) and an FKBP12 tag on the other monomer (FKBP12-Dyn). FRB and FKBP12 form a heterodimer in the presence of the small molecule rapamycin (Banaszynski et al., 2005). A C-terminal HaloTag (Promega) was used to fluorescently label dynein.

FRB-Dyn constructs carrying ATPase mutations, $AAA1_{E/Q}$ (E1849Q), $AAA3_{E/Q}$ (E2488Q) and monomeric Dyn $AAA1_{K/A}$ (K1802A), $AAA3_{K/A}$ (K2424A) were a generous gift of Ronald D. Vale (UCSF). An N-terminal FRB domain was added to the monomeric K/A mutants. FLH constructs were obtained by inserting an FRB or FKBP12 heterodimerization tag to the C-terminus of a Dyn construct carrying the appropriate ATPase mutations (Reck-Peterson et al., 2006). Assays on FRB-BLH dimerized to FKBP12-FLH or with FKBP12-BLH dimerized to FRB-FLH did not show a large difference in motor speed verifying that the speed measurements

are not affected by which tag is introduced to C- and N-terminus of the motor. Mutations to the yeast strains were carried out using homologous recombination.

Chimeric constructs which encode a monomeric *T. thermophilus* seryl-tRNA synthetase (SRS) and the dynein microtubule binding domain (MTBD) at different coiled-coil length and registry in a pET42a vector were generously provided by Ian Gibbons and Andrew P. Carter (Gibbons et al., 2005). A 4x(GS)-FKBP12 tag was inserted to the C-terminus of SRS by restriction digest and ligation. For optical trapping experiments, an eGFP gene was added in place of FKBP12. The SRS construct was additionally tagged with an N-terminal HaloTag for fluorescent labeling. Table 1 contains all of the constructs and their parent yeast strains used in this study.

Protein Expression, Purification and Labeling

Dynein proteins were expressed in yeast and purified as described (Reck-Peterson et al., 2006). Purified protein was stored in DLB (30 mM HEPES pH 7.2, 2 mM $MgCl_2$, 1 mM EGTA, 10% glycerol). Expression and purification of SRS-MTBD mutants were carried out in *E.coli,* as described [35].

For fluorescent tracking experiments, BLH heads containing a C-terminal HaloTag were labelled with 10μM TMR HaloTag ligand (Promega) for 1 h on ice during the protein preparation, prior to washing of the IgG beads (GE Healthcare).

SRS Chimera MT Co-sedimentation Assay

The SRS Chimera MT co-sedimentation assay (Figure 9) was carried out in DLB (30 mM HEPES pH 7.2, 2 mM $MgCl_2$, 1 mM EGTA, 10% glycerol) as described (Gibbons et al., 2005).

Microscope

Single-molecule motility assays were performed on a custom-built objective-type total internal reflection fluorescence (TIRF) microscope, equipped with an inverted microscope body (Nikon Ti-Eclipse) with perfect focusing system, 1.45 NA 60X microscope objective (Nikon, TIRF Plan Apochromat). The sample was illuminated with 488 nm and 532 nm solid state lasers (Coherent) to image GFP and TMR, respectively. BLH-TMR was imaged to record the speed and run length data, except in Supplementary Movie 1 in which SRS-TMR is imaged. FLH-GFP was imaged to confirm motility of the FLH (data not shown). For velocity assays, GST-Dyn motility was recorded with a 2 second exposure time under 5.1 mW 532 nm laser exposure. For run length assays, GST-Dyn motility was recorded under 1.9 mW of 532 nm illumination. Laser power and the image acquisition rate were adjusted for other constructs to keep the average distance traveled by motors (~100 nm per image) and the bleaching decay rate of TMR (0.004 per image) constant. Run length assays were done in buffer containing a final concentration of 75 mM K^+. Emitted photons were detected by an electron-multiplied charge-coupled device (EM-CCD) camera (Andor Ixon, 512x512 pixels, 16 μm pixel size). The image was magnified by a tube lens to obtain 129.3 nm effective pixel size, calibrated with a reticle containing 100 lines per mm.

Single-Molecule Motility Assays

Motility assays were performed as described (Reck-Peterson et al., 2006). Sea urchin axonemes were immobilized on a glass coverslip in a flow camber constructed with double sided tape. The

chamber was washed with 50 µl of DLB (30 mM HEPES pH 7.2, 2 mM $MgCl_2$, 1 mM EGTA, 10% glycerol), followed by 50 µl of DLBC (DLB with 1 mg/ml casein, 2 mM DTT). 200 pM dynein was then perfused into the chamber in DLBC and allowed to bind to MT for 1 minute. The flow cell was then washed with 100 µl of DLBC and 20 µl of imaging buffer (DLBC with 1% β-mercaptoethanol, 2 mM ATP, and an oxygen scavenging system consisting of 25 mM PCA, 0.35 mg/ml PCD, 0.6 mM Trolox (Rasnik et al., 2006)).

For assays of FRB-FKBP12 heterodimers, 1 µl of 600 nM rapamycin and a total volume of 2 µl of equimolar amounts of FRB- and FKBP12-tagged monomers were mixed and incubated in DLB for 10 minutes at room temperature. These constructs were then further diluted in DLBC before introducing the motor to sample chamber. 100 nM rapamycin was added to all assay buffers to maintain the dimerization. We are confident that the motility observed was due to heterodimerization because: (1) Under the motor concentrations used, we did not observe motility in the presence of only one type of the FRB- or FKBP12-tagged monomers. (2) Processive motility of FRB and FKBP12-tagged monomers was also not observed in the absence of rapamycin. (3) Selective ATPase mutations on BLH and FLH resulted in dramatic changes in dynein motility, depending on which head carried the mutation, which would not be possible if the motors observed were not heterodimers. (4) Fluorescently-labeled SRS chimeras are observed to be motile when heterodimerized with unlabeled dynein monomers. Fluorescent spots of individual quantum dots were localized with a two-dimensional Gaussian tracking algorithm. Trajectories of dyneins were fitted by a custom-written step finder algorithm, based on Schwartz Information Criterion (Kalafut and Visscher, 2008).

Gliding Assays

Gliding assays were performed as described previously(Reck-Peterson et al., 2006). Anti-GFP antibodies (~400 µg/ml) were added to a flow chamber constructed with double sided tape. The chamber was washed with 30 µl of buffer (either DLBCT (DLBC with 10 µM Taxol) or BRB80CT (80 mM PIPES pH 6.8, 1mM MgCl2, 1 mM EGTA, 100 mM KCl, 1 mg/ml casein, 2 mM DTT and 10 µM Taxol)). 20 µl of 2 µM of dynein was added to the flow chamber and allowed to bind antibodies for 30 seconds. The chamber was then washed with 30 µl of buffer. TMR labeled polarity-marked microtubules were flowed to the chamber and allowed to bind to dynein for 2 minutes. The chamber was then washed with 100 µl of buffer. 30 µl of imaging buffer (buffer with 1 mM ATP, and the oxygen scavenging system as in the single molecule assays, without trolox) containing the desired KCl concentration was flowed to the chamber.

Polarity-marked microtubules used in gliding assays were prepared by polymerizing brightly-labeled seeds by incubating 0.5 mg/ml TMR-tubulin and 1 mg/ml unlabeled tubulin in BRB80CT with 10% DMSO and 1 mM GTP, without DTT or casein, for 10 min at 37°C. 1.5 µl of seeds were added to a mixture containing 0.1 mg/ml TMR-tubulin, 2 mg/ml unlabeled tubulin, and 2 mg/ml NEM-modified tubulin in BRB80CT with 10% DMSO and 1 mM GTP, without DTT or casein, and incubated for 15 min at 37°C, 20 µl of BRB80CT, without casein was then added, and the mixture was incubated for an additional 15 min at 37°C. NEM-modified tubulin was prepared by mixing 100 µl of 5 mg/ml tubulin with 2 µl of 100 mM NEM (N-ethylmaleimide Thermo Scientific #23030) for 5 min at RT. After incubation 1 µl of 1 M DTT (dithiothreitol) was added and the mixture was incubated for 30 min on ice. Finally the sample was spun for 15 min at 80,000 rpm in a Beckmann-Coulter TLA 120 rotor for 15 min, the

supernatant was aliquoted, frozen in liquid nitrogen and stored at -80 °C. Tubulin was prepared from porcine brain.

Dynein MT-Release Under Flow

Sea urchin axonemes were immobilized on a glass coverlsip in a flow camber which allows buffer exchange while the chamber was mounted to the microscope stage (Figure 4). Axonemes were decorated with 20 µl of ~15 nM monomeric TMR-labeled dynein in DLBC without ATP and washed twice with DLBC to remove excess motor. The sample then washed with imaging buffer, which does not contain ATP, and TMR fluorescence was monitored under TIRF illumination. MT-bound dynein motors were monitored for 100 frames at 280 ms temporal resolution before exchanging the assay solution with imaging buffer plus nucleotide. The percentage of released dynein monomers was quantified by taking the average TMR fluorescence intensity along 5 MTs per movie (3 movies per nucleotide condition) for 10 s before and after flow, and by subtracting the background intensity from TMR fluorescence. The change in intensity before and after flow was normalized by the intensity before flow. The reduction of fluorescence intensity was not due to permanent photobleaching of TMR, which is minimal on the timescale of our experimental conditions, as confirmed by repeating the flow experiment in the absence of nucleotide.

Optical Trapping Assay

A custom-built optical trap consisting of a 2 W 1064 nm continuous wave laser (Coherent), a Nikon Ti-Eclipse microscope body and a Nikon 100x 1.49 NA Plan-Apo objective was used to study force-induced release of dynein monomers. To apply forces through the N-terminal linker of dynein, GFP-tagged dynein monomers were diluted in DLBC and incubated with carboxylated polystyrene beads (0.86 µm diameter, Invitrogen) coated with a rabbit polyclonal anti-GFP antibody (Covance). Antibody coating of the beads were carried out by EDC-NHS crosslinking (Pierce) (Gennerich et al., 2007). The motor-bead mixture was then diluted 10 fold in DLBC with 5 mg/ml casein, the PCA/PCD oxygen scavenging system and 2 mM ATP. For no nucleotide conditions, no additional ATP was added the motor bead-mixture, resulting in residual ATP concentrations of ~40 nM, well below dynein's $K_{M,\ ATP}$ of ~26 µM (Cho et al., 2008). The final bead concentration was 0.1% weight/volume. To record data from single monomers, motors were diluted to a level where we observed 5-15% binding probability during the oscillation of the beads. >90% of the binding events terminated with a single release step, indicative of binding of a single dynein monomer. At 10-fold higher motor concentrations, significant increase in multiple release events was observed (data not shown), while no events were observed in the absence of motor.

To apply forces through the C-terminal ring domain, dynein monomers with a C-terminal DHA-tag were labeled with a short (74 bp) double-stranded DNA strand. Two complimentary DNA strands, one with a 5'-biotin modification (5'-Biotin-TTCGGTCAATACCCGGCGCAGAGCGCTCAGGCGCGAGGTCAACAGAGGGCGGAGGG TGGGCCAGCGCGACCCCG-3'), the other with a 5'-amine modification (5'-AmMC6-GTGTCGGGGTCGCGCTGGCCCACCCTCCGCCCTCTGTTGACCTCGCGCCTGAGCGCT CTGCGCCGGGTATTGAC-3') (IDT) were hybridized by combining 30 µl of each strand from 100 µM stock with 20 µl of DNA buffer (80 mM $NaHCO_3$ pH 8.4, 200 mM KCl, 5 mM $MgCl_2$), heating at 90ºC for 20 minutes, cooling to 25ºC for 40 minutes. The DNA mixture was then

reacted with 160 μM HaloTag NHS ligand (Promega) for 6 h at room temperature and the reaction quenched with 1 μl of 1 M glycine, pH 8.4. DNA was then desalted through G-25 spin columns into DNA buffer. Dynein (~400 μl) was then labeled with the purified HaloTag-DNA-biotin for 6 h on ice, and excess DNA was removed through microtubule bind and release purification[33]. This dynein-DNA-biotin complex was then incubated with streptavidin coated polystyrene beads (0.86 μm diameter, Invitrogen), as described above. The motor-bead mixture was then diluted in the imaging buffer.

Cy5-labeled axonemes were adsorbed to the surface of a flow cell prior to addition of the bead/dynein mixture. The sample was excited with 633 nm HeNe laser (Melles Griot) and axonemes were visualized with a CCD camera. The trapping beam was steered by two computer-controlled acousto-optical deflectors (AOD's) (AA Electronics) to capture and position floating monodisperse beads. Trap stiffness was calibrated for each sample by fitting the windowed power spectrum of a bead trapped 3 μm above the surface of the coverslip to a Lorentzian curve[51]. The microspheres were trapped by a ~50 mW 1064 nm laser beam to achieve a spring constant of ~0.05 pN/nm. A position sensitive detector (PSD) was located at the back focal plane to detect microsphere displacement. The PSD data was recorded at 20 kHz for calibration and 5 kHz for data acquisition. The response of the PSD was calibrated in each sample by rapidly scanning the laser across a trapped bead in both x and y directions using the AOD's and fitting the resulting curve to a cubic polynomial. This calibration was repeated once at the surface and once 3 μm into the solution to avoid systematic errors in either experimental data or stiffness calibrations.

Trapped beads were positioned over a Cy5-labeled axoneme and oscillated between two positions (± 125 nm) along the long axis of the axoneme. Bead-trap separation was monitored in real time to prevent trap oscillations during a binding event. The trap was held steady for 0.25 s after the bead returned to the trap center, and then moved to the opposite position. Microtubule polarity was determined by imaging Oregon green labeled kinesin motors, which decorate the plus end of MTs. GFP-labeled kinesin was used in trapping experiments on DNA-tethered dynein monomers, which lack GFP. Strong (3-10 fold) asymmetry was observed in the release rate of both linker and C-terminal bound dynein monomers in the presence of ATP (all of 11 axonemes tested) (data not shown). The rest of the data was collected by assigning the microtubule polarity based on the asymmetry in the plus and minus-end directed release rates of dynein monomers.

Data Analysis

The kymographs of GFP-tagged dyneins were made in ImageJ. To monitor the run lengths of single motors, we only analyzed molecules which moved at least 4 pixels (~500 nm), began their runs at least 5 μm away from the minus end of MTs and at least 50 frames before the end of the movie. Since the average distance traveled by a motor before photobleaching (25 μm) is much greater than the measured average run length (0.8-2.2 μm), we have not included a correction for photobleaching in our analysis. Such a correction would result in an increase of run length of less than 5%, within the error of our measurement. The mean run length was calculated by maximum likelihood estimation of the exponential decay constant, stated errors are the 95% confidence intervals.

In optical trap assays, single step MT release events were analyzed and rare multiple step release events were discarded from the data analysis. Load-induced MT release data was fit with a custom step finding algorithm which fits the trap position data during each period of oscillation to two steps. Events showing a dwell time of greater than 2.5 ms were evaluated visually to confirm the binding and release of a single monomer. The applied force to the motor was calculated by trap stiffness and the bead-trap separation vector. Data consisting of applied force and dwell time were sorted by force and binned every 100 data points. The dwell times in each bin were fit to a single exponential decay (see Figure 10C, inset), and resulting rate constant was plotted with the average force of all the data points in the bin. Errors are the 95% confidence intervals. Changing the bin size did not significantly affect the results (not shown).

Computational Model

Monte Carlo simulations were run to generate stepping traces of a WT dynein dimer. The model incorporates parameters from bulk ATPase (Cho et al., 2008; Reck-Peterson et al., 2006), optical trap and stepping measurements (DeWitt et al., 2012; Qiu et al., 2012) of yeast dynein (see below).

The model assumes ATP-dependent steps can occur when the interhead separation is less than 20 nm. Each head can step with a rate k_1 (8 s^{-1} for WT motors, 0.6 s^{-1} for $AAA3_{E/Q}$ mutants, and 0 for FLH and AAA1 mutants), based on bulk ATPase measurements per head (Cho et al., 2008; Reck-Peterson et al., 2006). The stepping head rebinds the MT at a position randomly chosen from a Gaussian distribution with a mean 8 ± 16 nm (± S.D.) towards the minus from its partner head. The 8 nm minus end directed bias in step size is provided by the ATP-dependent linker swing mechanism (Roberts et al., 2009). FLH_{WT} and $AAA1_{E/Q}$ mutants, which lack the ability to generate a powerstroke, undergo non-productive ATP-dependent stepping with a rate k_2 = ~20 s^{-1}, rebinding at a position randomly chosen from a Gaussian distribution centered at its partner head with 0 ± 16 nm (SD) step size**.** This feature models the constitutive weakly bound state observed for $AAA1_{E/Q}$ mutants, and C-terminally bound WT monomers (Figure 12C).

Tension dependent steps occur when the interhead separation is greater than 12 nm. In this mode of stepping, the leading head steps backwards with a rate k_3 (determined from optical trap data) (Figures 10 and 17). The trailing head steps with a rate $k_4 = mx$, where x is the interhead separation in nm, k_4 is determined from optical trap data (Figures 10 and 17), corresponding to the release rate at 0 pN of force. Tension induced stepping rate increases at higher interhead separations (due to increase in intramolecular tension). *m* was calculated from linear fits to the force-induced release data (Figures 10 and 17). Fixing the release rate to be equal to the rate measured for a 1-3 pN bin of force data at all interhead separations did not significantly affect the speeds of any of the mutants (data not shown). After a tension based step, the motor rebinds the MT at a position randomly chosen from a Gaussian distribution, 8 ± 16 nm from its partner head in the direction of the initial position of the stepping head. When the heads are between 12 and 20 nm apart, both tension dependent and independent steps are possible. At separations higher than 20 nm, the ATP dependent stepping mechanism is abolished due to the increased tension on the linker domain (Figures 10C, D). Excluding tension independent steps in this state did not significantly affect the results.

200 simulations were run for 100 s with a time step of 0.005 s to estimate the speed of each construct. In simulations of mutant dyneins, C- and N-terminal pulling data were used to calculate the force induced release rates of FLH and BLH.

Monte Carlo Simulations

The model is defined by parameters that determine the size and distribution of the steps, and the interhead separations at which tension begins and at which ATP-dependent release is inhibited, and by the rates at which these steps take place. The model simulates different mutants described in this paper. Each mutant dynein monomer has an associated set of rates measured from our optical trapping assay and reported ATPase rates. Mutants seen to release MTs under no tension in the presence of ATP (Figure 4) (AAA1 E/Q and FLH) undergo MT release without powerstroke stepping, rebinding the MT at a random location centered around the non-stepping head. The python code used in the simulations is available at http://physics.berkeley.edu/research/yildiz/SubPages/code_repository.html.

The following parameters were used to define the geometry of the model:

- distwidth: the s.d. of the stepping distribution for both tension-dependent and powerstroke stepping (16 nm).
- fwdbias: forward bias of landing site, in front of non-stepping head, during powerstroke stepping (8 nm).
- tstart: distance (head to head separation) at which tension based stepping begins (12 nm)
- diffstop: distance (head to head separation) at which powerstroke steps stop (20 nm)
- tensionbias: the average distance, from partner head, that a tension stepping head will land (8 nm)

Rates, except for powerstroke rates, which are reported ATPase rates, are derived from linear fits to our optical trapping assay. The values used are shown in Supplementary Table 2.

- atprelease: release of a head from the MT due to ATP binding (powerstroke stepping). From reported ATPase rates.
- tstepback: release of a head due to tension when the head leads. Calculated from the average value of the release rates measured under (+)-end directed force.
- nodirrelase: release of a head due to weak MT binding. Measured from the y-intercept (0-force value) of the linear fit to release rates measured under (+)-end directed force.
- tstepforwint: y-intercept (interhead separation = 0) value of the line defining head release as a function of interhead separation when the head trails
- tstepforslope: slope value of the line fit to release rates measured under (-)-end directed force.

For each dwell of the motor, the tension-based rate for the trailing head was recalculated according to the fit line of the optical trap data, and the assumed stiffness of the linkage between monomers (1/12 pN/nm) (Figure 18). The heads vary by their attachment geometry (BLH heads corresponding to linker bound trapping assays, FLH heads corresponding to C-terminal trapping

assays) and ATPase mutations). We used the rates for each construct as shown in (Table 2 and Figure 17).

For each mutant simulated, the name of the mutant and two heads making up the mutant heterodimer are shown in Table 3.

Tables

Construct	Genotype	Source
VY1	MATa *his3-1,15 ura3-1 leu2-3,112; ade2-1; trp1-1; can1-100*	(Eshel et al., 1993)
VY2	*dyn1Δ::HIS3*	(Eshel et al., 1993)
VY207	*pep4::HIS3 prb1Δ pGAL-ZZ-TEV-3XHA-FKBP-331DYN1-gs-DHA*	(Reck-Peterson et al., 2006)
VY208	*pep4::HIS3 prb1Δ pGAL-ZZ-TEV-GFP-3XHA-GST-331DYN1-gs-DHA1*	(Reck-Peterson et al., 2006)
VY209	*pep4::HIS3 prb1Δ pGAL-ZZ-TEV-3XHA-FRB-331DYN1-gs-DHA*	(Reck-Peterson et al., 2006)
VY268	*pep4::HIS3 prb1Δ PAC11-13MYC::TRP ZZ-TEV-DHA-GST-331*	(Reck-Peterson et al., 2006)
VY323	*pep4::HIS3 prb1Δ PAC11-13XMYC::TRP pGAL-ZZ-TEV-GFP-3XHA-331DYN1-gsgsgsgs-GST*	(Reck-Peterson et al., 2006)
Y128	*pep4::HIS5 prb1Δ pGAL-ZZ-TEV-FRB-331DYN1-K1802A-gs-DHA*	This study
VY543	*pep4::HIS5 prb1Δ pGAL-ZZ-TEV-FRB-331DYN1-E1849Q-gs-DHA*	R.D. Vale
Y127	*pep4::HIS5 prb1Δ pGAL-ZZ-TEV-FRB-331DYN1-K2424A-gs-DHA*	This study
VY549	*pep4::HIS5 prb1Δ pGAL-ZZ-TEV-FRB-331DYN1-E2488Q-g-sDHA*	R.D. Vale
Y138	*pep4::HIS3 prb1Δ PAC11-13XMYC::TRP pGAL-ZZ-TEV-GFP-3XHA-331DYN1-gsgsgsgs-FRB URA3*	This study
Y144	*pep4::HIS3 prb1Δ PAC11-13XMYC::TRP pGAL-ZZ-TEV-GFP-3XHA-331DYN1-gsgsgsgs-FKBP12 URA3*	This study
Y155	*pep4::HIS5 prb1Δ pGAL-ZZ-TEV-GFP-3XHA-331DYN1-K1802A-gsgsgsgs-FRB URA3*	This study
Y150	*pep4::HIS3 prb1Δ PAC11-13XMYC::TRP pGAL-ZZ-TEV-GFP-3XHA-331DYN1-E1849Q-gsgsgsgs-FKBP12 URA3*	This study
Y156	*pep4::HIS5 prb1Δ pGAL-ZZ-TEV-GFP-3XHA-331DYN1-K2424A-gsgsgsgs-FRB URA3*	This study
Y154	*pep4::HIS3 prb1Δ PAC11-13XMYC::TRP pGAL-ZZ-TEV-GFP-3XHA-331DYN1(E2488Q)-gsgsgsgs-FKBP12 URA3*	This study
Y167	*pep4::HIS3 prb1Δ pGAL-ZZ-TEV-3XHA-FRB-331DYN1-gs-DHA ZZ-TEV-GFP-3XHA-GST-D6(MTBD replaced with FRB)-gs-DHA*	This Study

CY29	*MATa his3-11,5 ura3-1 leu2-3,112 ade2-1 trp-1 pep4::HIS5 prb1Δ pGal-ZZ-Tev-GFP-HA-331DYN-URA3$_{K.lactis}$-331DYN-gsDHA*	This study
CY40	*MATa his3-11,5 ura3-1 leu2-3,112 ade2-1 trp-1 pep4::HIS5 prb1Δ pGal-ZZ-Tev-GFP-3xHA-GST-331DYN-URA3$_{K.lactis}$-331DYN-gsDHA*	This study
CY134	*MATa his3-11,5 ura3-1 leu2-3,112 ade2-1 trp-1 pep4::HIS5 prb1Δ pGal-ZZ-Tev-GFP-3xHA-GST-$_{AAA1E/Q}$331DYN-URA3$_{K.lactis}$-331DYN-gsDHA*	This study
CY151	*MATa his3-11,5 ura3-53 leu2-3,112 ade2-1 trp-1 pep4::HIS5 pGal-ZZ-Tev-GFP-3xHA-GST-$_{AAA1E/Q}$331DYN$_{L3034}$-colicin-K322-gs-colicin-$_{I3293}$331DYN-gsDHA*	This study
CY379	*MATa his3-11,5 ura3-1 leu2-3,112 ade2-1 trp-1 pep4::HIS5 prb1Δ pGal-ZZ-Tev-GFP-3xHA-GST-331DYN$_{L3034}$-colicin-K322$_{R203K}$-gs-colicin-$_{I3293}$331DYN-gsDHA*	This study
CY384	*MATa his3-11,5 ura3-1 leu2-3,112 ade2-1 trp-1 pep4::HIS5 prb1Δ pGal-ZZ-Tev-GFP-3xHA-GST-$_{AAA1E/Q}$331DYN$_{L3034}$-colicin-K322$_{R203K}$-gs-colicin-$_{I3293}$331DYN-gsDHA*	This study
CY399	*MATa his3-11,5 ura3-52 leu2-3,112 ade2-1 trp-1 pep4::HIS5 prb1Δ pGal-ZZ-Tev-GFP-HA-331DYN$_{L3034}$-colicin-K322$_{R203K}$-gs-colicin-$_{I3293}$331DYN*	This study
CY412	*MATa his3-11,5 ura3-1 leu2-3,112 ade2-1 trp-1 pep4::HIS5 prb1Δ pGal-ZZ-Tev-GFP-3xHA-GST-331DYN$_{L3034}$-colicin-K322-gs-colicin-$_{I3293}$331DYN-gsDHA*	This study
CY413	*MATa his3-11,5 ura3-1 leu2-3,112 ade2-1 trp-1 pep4::HIS5 prb1Δ pGal-ZZ-Tev-GFP-3xHA-GST-331DYN$_{Q3083}$-colicin-K322$_{R203K}$-gs-colicin-$_{K3244}$331DYN-gsDHA*	This study
pFC5	SRS-dynein stalk MTBD fusion (22:19), pET42a vector	(Gibbons et al., 2005)

pFC7	SRS-dynein stalk MTBD fusion (85:82), pET42a vector	(Gibbons et al., 2005)
pFC8	SRS-dynein stalk MTBD fusion (89:82), pET42a vector	(Gibbons et al., 2005)
pFC9	SRS-dynein stalk MTBD (22:19)-FKBP12	This study
pFC11	SRS-dynein stalk MTBD (85:82)-FKBP12	This study
pFC12	SRS-dynein stalk MTBD (89:82)-FKBP12	This study
pFC15	SRS-dynein stalk MTBD (85:82)-GFP	This study
pFC21	HaloTag-SRS-dynein stalk MTBD (85:82)-FKBP12	This study

Table 1. The list of yeast strains (Y- numbered) and SRS-MTBD chimera plasmids (pFC-numbered) used in this study.

head	**tstepback**	**nodirrelease**	**tstepforwint**	**tstepforwslope**	**atprelease**
C-term AAA1$_{E/Q}$	23.2	22.5	3.18	0.88	0
C-term AAA3$_{E/Q}$	1.56	1.73	0.80	0.14	0
C-term WT	15.5	15.6	12.0	0.64	0
Linker AAA3$_{E/Q}$	2.6	2.37	1.64	0.29	0.6
Linker WT	1.56	1.19	-0.35	0.27	8

Table 2. Rates used in the model (all values in 1/s).

Mutant	**Head 1**	**Head 2**
BLH-BLH	Linker WT	Linker WT
BLH-FLH	Linker WT	C-term WT
BLH-FLH$_{AAA1\ E/Q}$	Linker WT	C-term AAA1$_{E/Q}$
BLH-FLH$_{AAA3\ E/Q}$	Linker WT	C-term AAA3$_{E/Q}$
BLH$_{AAA3\ E/Q}$-BLH	Linker AAA3$_{E/Q}$	Linker WT
BLH$_{AAA3\ E/Q}$-FLH	Linker AAA3$_{E/Q}$	C-term WT

Table 3. Mutant heterodimers simulated with the computational model.

References

Ananthanarayanan, V., Schattat, M., Vogel, S.K., Krull, A., Pavin, N., and Tolić-Nørrelykke, I.M. (2013). Dynein motion switches from diffusive to directed upon cortical anchoring. Cell *153*, 1526–1536.

Asbury, C.L., Fehr, A.N., and Block, S.M. (2003). Kinesin moves by an asymmetric hand-over-hand mechanism. Science *302*, 2130–2134.

Banaszynski, L.A., Liu, C.W., and Wandless, T.J. (2005). Characterization of the FKBP.rapamycin.FRB ternary complex. J. Am. Chem. Soc. *127*, 4715–4721.

Block, S.M. (2007). Kinesin motor mechanics: binding, stepping, tracking, gating, and limping. Biophys. J. *92*, 2986–2995.

Bryant, Z., Altman, D., and Spudich, J. a (2007). The power stroke of myosin VI and the basis of reverse directionality. Proc. Natl. Acad. Sci. U. S. A. *104*, 772–777.

Burgess, S.A., Walker, M.L., Sakakibara, H., Knight, P.J., and Oiwa, K. (2003). Dynein structure and power stroke. Nature *421*, 715–718.

Carminati, J.L., and Stearns, T. (1997). Microtubules orient the mitotic spindle in yeast through dynein-dependent interactions with the cell cortex. J. Cell Biol. *138*, 629–641.

Carter, A.P., Garbarino, J.E., Wilson-Kubalek, E.M., Shipley, W.E., Cho, C., Milligan, R. a, Vale, R.D., and Gibbons, I.R. (2008). Structure and functional role of dynein's microtubule-binding domain. Science *322*, 1691–1695.

Carter, A.P., Cho, C., Jin, L., and Vale, R.D. (2011). Crystal structure of the dynein motor domain. Science *331*, 1159–1165.

Cho, C., Reck-Peterson, S.L., and Vale, R.D. (2008). Regulatory ATPase sites of cytoplasmic dynein affect processivity and force generation. J. Biol. Chem. *283*, 25839–25845.

Clancy, B.E., Behnke-Parks, W.M., Andreasson, J.O.L., Rosenfeld, S.S., and Block, S.M. (2011). A universal pathway for kinesin stepping. Nat. Struct. Mol. Biol. *18*, 1020–1027.

DeWitt, M. a, Chang, A.Y., Combs, P. a, and Yildiz, A. (2012). Cytoplasmic dynein moves through uncoordinated stepping of the AAA+ ring domains. Science *335*, 221–225.

Dunn, A.R., Chuan, P., Bryant, Z., and Spudich, J. a (2010). Contribution of the myosin VI tail domain to processive stepping and intramolecular tension sensing. Proc. Natl. Acad. Sci. U. S. A. *107*, 7746–7750.

Gee, M.A., Heuser, J.E., and Vallee, R.B. (1997). An extended microtubule-binding structure within the dynein motor domain. Nature *390*, 636–639.

Gennerich, A., and Vale, R.D. (2009). Walking the walk: how kinesin and dynein coordinate their steps. Curr. Opin. Cell Biol. *21*, 59–67.

Gennerich, A., Carter, A.P., Reck-peterson, S.L., and Vale, R.D. (2007). Force-Induced Bidirectional Stepping of Cytoplasmic Dynein. Cell 952–965.

Gerdes, J.M., and Katsanis, N. (2005). Microtubule transport defects in neurological and ciliary disease. Cell. Mol. Life Sci. *62*, 1556–1570.

Gibbons, I.R., Garbarino, J.E., Tan, C.E., Reck-Peterson, S.L., Vale, R.D., and Carter, A.P. (2005). The affinity of the dynein microtubule-binding domain is modulated by the conformation of its coiled-coil stalk. J. Biol. Chem. *280*, 23960–23965.

Griffis, E.R., Stuurman, N., and Vale, R.D. (2007). Spindly, a novel protein essential for silencing the spindle assembly checkpoint, recruits dynein to the kinetochore. J. Cell Biol. *177*, 1005–1015.

Hafezparast, M., Klocke, R., Ruhrberg, C., Marquardt, A., Ahmad-Annuar, A., Bowen, S., Lalli, G., Witherden, A.S., Hummerich, H., Nicholson, S., et al. (2003). Mutations in dynein link motor neuron degeneration to defects in retrograde transport. Science *300*, 808–812.

Huang, J., Roberts, A.J., Leschziner, A.E., and Reck-Peterson, S.L. (2012). Lis1 acts as a "clutch" between the ATPase and microtubule-binding domains of the dynein motor. Cell *150*, 975–986.

Imamula, K., Kon, T., Ohkura, R., and Sutoh, K. (2007). The coordination of cyclic microtubule association/dissociation and tail swing of cytoplasmic dynein. Proc. Natl. Acad. Sci. U. S. A. *104*, 16134–16139.

Kalafut, B., and Visscher, K. (2008). An objective, model-independent method for detection of non-uniform steps in noisy signals. Comput. Phys. Commun. *179*, 716–723.

Kardon, J.R., and Vale, R.D. (2009). Regulators of the cytoplasmic dynein motor. Nat. Rev. Mol. Cell Biol. *10*, 854–865.

Kaseda, K., Higuchi, H., and Hirose, K. (2003). Alternate fast and slow stepping of a heterodimeric kinesin molecule. Nat. Cell Biol. *5*, 1079–1082.

Klumpp, L.M., Mackey, A.T., Farrell, C.M., Rosenberg, J.M., and Gilbert, S.P. (2003). A kinesin switch I arginine to lysine mutation rescues microtubule function. J. Biol. Chem. *278*, 39059–39067.

Kon, T., Nishiura, M., Ohkura, R., Toyoshima, Y.Y., and Sutoh, K. (2004). Distinct functions of nucleotide-binding/hydrolysis sites in the four AAA modules of cytoplasmic dynein. Biochemistry *43*, 11266–11274.

Kon, T., Mogami, T., Ohkura, R., Nishiura, M., and Sutoh, K. (2005). ATP hydrolysis cycle-dependent tail motions in cytoplasmic dynein. Nat. Struct. Mol. Biol. *12*, 513–519.

Kon, T., Imamula, K., Roberts, A.J., Ohkura, R., Knight, P.J., Gibbons, I.R., Burgess, S.A., and Sutoh, K. (2009). Helix sliding in the stalk coiled coil of dynein couples ATPase and microtubule binding. Nat. Struct. Mol. Biol. *16*, 325–333.

Kon, T., Sutoh, K., and Kurisu, G. (2011). X-ray structure of a functional full-length dynein motor domain. Nat. Struct. Mol. Biol. *18*, 638–642.

Kon, T., Oyama, T., Shimo-Kon, R., Imamula, K., Shima, T., Sutoh, K., and Kurisu, G. (2012). The 2.8 Å crystal structure of the dynein motor domain. Nature *484*, 345–350.

Mallik, R., Carter, B.C., Lex, S.A., King, S.J., and Gross, S.P. (2004). Cytoplasmic dynein functions as a gear in response to load. Nature *427*, 649–652.

McKenney, R.J., Vershinin, M., Kunwar, A., Vallee, R.B., and Gross, S.P. (2010). LIS1 and NudE induce a persistent dynein force-producing state. Cell *141*, 304–314.

Morales-Mulia, S., and Scholey, J.M. (2005). Spindle pole organization in Drosophila S2 cells by dynein, abnormal spindle protein (Asp), and KLP10A. Mol. Biol. Cell *16*, 3176–3186.

Nicastro, D., Schwartz, C., Pierson, J., Gaudette, R., Porter, M.E., and McIntosh, J.R. (2006). The molecular architecture of axonemes revealed by cryoelectron tomography. Science *313*, 944–948.

Nishiura, M., Kon, T., Shiroguchi, K., Ohkura, R., Shima, T., Toyoshima, Y.Y., and Sutoh, K. (2004). A single-headed recombinant fragment of Dictyostelium cytoplasmic dynein can drive the robust sliding of microtubules. J. Biol. Chem. *279*, 22799–22802.

Oda, T., Hirokawa, N., and Kikkawa, M. (2007). Three-dimensional structures of the flagellar dynein-microtubule complex by cryoelectron microscopy. J. Cell Biol. *177*, 243–252.

Ori-McKenney, K.M., Xu, J., Gross, S.P., and Vallee, R.B. (2010). A cytoplasmic dynein tail mutation impairs motor processivity. Nat. Cell Biol. *12*, 1228–1234.

Qiu, W., Derr, N.D., Goodman, B.S., Villa, E., Wu, D., Shih, W., and Reck-Peterson, S.L. (2012). Dynein achieves processive motion using both stochastic and coordinated stepping. Nat. Struct. Mol. Biol.

Rai, A.K., Rai, A., Ramaiya, A.J., Jha, R., and Mallik, R. (2013). Molecular adaptations allow dynein to generate large collective forces inside cells. Cell *152*, 172–182.

Rasnik, I., McKinney, S.A., and Ha, T. (2006). Nonblinking and long-lasting single-molecule fluorescence imaging. Nat. Methods *3*, 891–893.

Reck-Peterson, S.L., Yildiz, A., Carter, A.P., Gennerich, A., Zhang, N., and Vale, R.D. (2006). Single-molecule analysis of dynein processivity and stepping behavior. Cell *126*, 335–348.

Redwine, W.B., Hernandez-Lopez, R., Zou, S., Huang, J., Reck-Peterson, S.L., and Leschziner, a. E. (2012). Structural Basis for Microtubule Binding and Release by Dynein. Science (80-.). *337*, 1532–1536.

Roberts, A.J., Numata, N., Walker, M.L., Kato, Y.S., Malkova, B., Kon, T., Ohkura, R., Arisaka, F., Knight, P.J., Sutoh, K., et al. (2009). AAA+ Ring and linker swing mechanism in the dynein motor. Cell *136*, 485–495.

Ross, J.L., Wallace, K., Shuman, H., Goldman, Y.E., and Holzbaur, E.L.F. (2006). Processive bidirectional motion of dynein-dynactin complexes in vitro. Nat. Cell Biol. *8*, 562–570.

Sablin, E.P., Case, R.B., Dai, S.C., Hart, C.L., Ruby, A., Vale, R.D., and Fletterick, R.J. (1998). Direction determination in the minus-end-directed kinesin motor ncd. Nature *395*, 813–816.

Sakakibara, H., Kojima, H., Sakai, Y., Katayama, E., and Oiwa, K. (1999). Inner-arm dynein c of Chlamydomonas flagella is a single-headed processive motor. Nature *400*, 586–590.

Sasaki, S., Shionoya, A., Ishida, M., Gambello, M.J., Yingling, J., Wynshaw-Boris, A., and Hirotsune, S. (2000). A LIS1/NUDEL/cytoplasmic dynein heavy chain complex in the developing and adult nervous system. Neuron *28*, 681–696.

Schmidt, H., Gleave, E.S., and Carter, A.P. (2012). Insights into dynein motor domain function from a 3.3-Å crystal structure. Nat. Struct. Mol. Biol. *19*, 492–497.

Shastry, S., and Hancock, W.O. (2010). Neck linker length determines the degree of processivity in kinesin-1 and kinesin-2 motors. Curr. Biol. *20*, 939–943.

Shima, T., Kon, T., Imamula, K., Ohkura, R., and Sutoh, K. (2006a). Two modes of microtubule sliding driven by cytoplasmic dynein. Proc. Natl. Acad. Sci. U. S. A. *103*, 17736–17740.

Shima, T., Imamula, K., Kon, T., Ohkura, R., and Sutoh, K. (2006b). Head-head coordination is required for the processive motion of cytoplasmic dynein, an AAA+ molecular motor. J. Struct. Biol. *156*, 182–189.

Thoresen, T., and Gelles, J. (2008). Processive movement by a kinesin heterodimer with an inactivating mutation in one head. Biochemistry *47*, 9514–9521.

Uemura, S., and Ishiwata, S. (2003). Loading direction regulates the affinity of ADP for kinesin. Nat. Struct. Biol. *10*, 308–311.

Uemura, S., Kawaguchi, K., Yajima, J., Edamatsu, M., Toyoshima, Y.Y., and Ishiwata, S. (2002). Kinesin-microtubule binding depends on both nucleotide state and loading direction. Proc. Natl. Acad. Sci. U. S. A. *99*, 5977–5981.

Vallee, R.B., Williams, J.C., Varma, D., and Barnhart, L.E. (2004). Dynein: An ancient motor protein involved in multiple modes of transport. J. Neurobiol. *58*, 189–200.

Vallee, R.B., McKenney, R.J., and Ori-McKenney, K.M. (2012). Multiple modes of cytoplasmic dynein regulation. Nat. Cell Biol. *14*, 224–230.

Yildiz, A., Forkey, J.N., McKinney, S.A., Ha, T., Goldman, Y.E., and Selvin, P.R. (2003). Myosin V walks hand-over-hand: single fluorophore imaging with 1.5-nm localization. Science *300*, 2061–2065.

Yildiz, A., Tomishige, M., Vale, R.D., and Selvin, P.R. (2004). Kinesin walks hand-over-hand. Science *303*, 676–678.

Yildiz, A., Tomishige, M., Gennerich, A., and Vale, R.D. (2008). Intramolecular strain coordinates kinesin stepping behavior along microtubules. Cell *134*, 1030–1041.